Long baseline navigation with explicit pseudo-range clock offset and propagation speed estimation

Pedro Batista

European Journal of Control, vol. 49, pp. 116-130, September 2019

https://doi.org/10.1016/j.ejcon.2018.12.010

Long Baseline Navigation with Explicit Pseudo-Range Clock Offset and Propagation Speed Estimation

Pedro Batista[a]

[a]*Institute for Systems and Robotics, Laboratory of Robotics and Engineering Systems, Instituto Superior Técnico, Universidade de Lisboa, Portugal*

Abstract

This paper proposes a novel one-way-travel-time (OWTT) long baseline (LBL) navigation concept that departs from previous approaches in that: i) the clock of the receiver in the vehicle needs not to be synchronized with the clocks of the emitters; and ii) the speed of propagation of the signals is assumed unknown. The nonlinear system dynamics are considered in a continuous-discrete time framework, taking advantage of the pseudo-range measurements obtained at low update rates and the data from other sensors obtained at high rates. An augmented system is proposed whose observability is analyzed and that is shown to be equivalent to the original nonlinear system under appropriate conditions. A Kalman filter provides the estimation solution, with globally exponentially stable error dynamics, in spite of the original nonlinear nature of the system dynamics. The performance of the proposed solution is evaluated with numerical simulations resorting to Monte Carlo runs. The comparison with the extended Kalman filter and the Bayesian Cramér-Rao bound are also included.

Key words: long baseline; navigation; clock offset; sound speed; one-way-travel-time.

1. Introduction

The global positioning system (GPS) is one of the most popular options when it comes to the choice of aiding devices for navigation purposes. However, in some scenarios, the GPS is unavailable, such as in underwater environments, where the attenuation that the electromagnetic waves suffer prevents its use, which fosters the development of alternative solutions. In underwater, long baseline (LBL) acoustic positioning systems have been widely explored, usually in one of two alternative modes: i) in one-way-travel-time (OWTT) LBL configurations, the clocks are assumed synchronized, the speed of propagation of the acoustic waves is assumed available, and the distances between several known emitters and the receiver installed on-board the vehicle are computed based on time tags that are sent along the acoustic signals; or ii) in two-way-travel-time (TWTT) LBL configurations, a transponder installed on-board the vehicle interrogates a set of known transponders that are fixed in the mission scenario and computes the distances between the vehicle and each of these transponders based on the round-trip travel time assuming that the speed of propagation of the acoustic signals is available.

Some of the early work on underwater acoustic positioning systems can be found in [1] and [2]. An extended Kalman filter (EKF) with a Rauch-Tung-Striebel smoother is implemented in [3] to solve the 2D navigation problem with three acoustic transponders. A conventional LBL positioning system is merged with a Doppler sonar, with bottom-lock, in [4]. It includes a magnetometer and roll/pitch sensors, and a complementary low-pass/high-pass filter approach is implemented to show that the Doppler precision is effectively improved. In [5] two different LBL alternatives are presented : i) fix computation approach; and ii) filtering approach. In the first, dead-reckoning is performed between acoustic fixes, which reset the vehicle position whenever available. In the second, dead-reckoning is performed but valid travel times are used, whenever available, to correct for dead-reckoning drift. In [6] some preliminary field trials are shown of a navigation system that consists of a LBL acoustic positioning system, a Doppler sonar, a fiber-optic North seeking gyro, pressure sensors and magnetic compasses, whereas the main navigation algorithm resorts to the least-squares method. In [7] the problem of navigation with pseudo-range measurements, considering additive bias, is addressed. The approach that is proposed therein is new in that it uses a three-stage filter. In particular, a linearized Kalman filter is proposed that avoids divergence as the linearization is made about estimates of another sub-optimal Kalman filter that is based on a valid quasi-linear measurement model. A similar approach is followed in [8] and [9] but considering a multiplicative unknown parameter, which accounts for the unknown wave speed. A different concept was proposed in [10], where one aims to estimate a segment of the trajectory instead of the current position. To that purpose, diffusion-based trajectory observers are considered. Another interesting setup was presented in [11], where distance measurements to a single acoustic source are considered, combined with dead-reckoning between distance measurements, to obtain a so-called synthetic long baseline. A related approach is proposed in [12], where simulations of a so-called virtual long baseline (VLBL) navigation algorithm for autonomous underwater vehicles are presented. In these two approaches some kind of trilateration is

Email address: pbatista@isr.tecnico.ulisboa.pt (Pedro Batista)

performed, even though not instantaneous. The direct use of distance measurements to a single source, without explicit trilateration, was evaluated in [13], where the distance measurements are fused with the data obtained from an inertial navigation system (INS) in an EKF. The topic of single range navigation has seen many contributions, see e.g. [14], [15], [16], [17], and [18]. Finally, in what concerns acoustic-based positioning and navigation systems, it is also important to refer the ultra-short baseline (USBL) acoustic positioning systems, which are rapidly increasing in popularity and number, see e.g. [19], [20], and references therein. For interesting discussions and detailed surveys on underwater vehicle navigation techniques and challenges, see [21], [22], and [23].

In OWTT navigation, the beacons and receiver clocks are assumed synchronized and the time of signal emission is either predefined or encoded and sent through communication modems, see [24], [25], and references therein. However, high-grade clocks must be employed, to mitigate clock drift, and clock synchronization at the beginning of each mission must be performed, which poses an additional and very heavy burden. Finally, even with high-grade clocks, clock drift is inevitable in long missions unless synchronization is performed periodically. On the other hand, a common assumption throughout the literature is that the speed of propagation of the waves in the medium is known or measured. This quantity depends on several characteristics such as the salinity, pressure, and temperature and it is either measured or profiled, often prior to the experiments. If that is not the case, or even for small errors of the sound velocity profile, the range measurements can carry large errors, particularly when the distances become large, thus putting into question the entire navigation data. While that is out of the scope of the paper, there exist many algorithms in the literature to handle the presence of outliers, see e.g. [14] and [26].

In previous work by the authors a novel filtering solution was proposed for LBL navigation [27] based on an extension of the framework for single range measurements detailed in [18]. In these approaches, the range measurements were assumed to be available, either resorting to two-way-travel-time or to OWTT coupled with synchronous clocks and acoustic communications. In short, the system dynamics are augmented, including as system states the range measurements and identifying nonlinear terms with new system states, until the system can be regarded as linear. A careful observability analysis follows and, due to its constructive nature, the Kalman filter provides the estimation solution with globally exponentially stable (GES) error dynamics. Previous works applying state augmentation to applications with LBL positioning can be found in [28], [29], and [30], where past measurements were included in the state. In the present work the differences between pseudo-range measurements are considered as additional states. More recently, in [31] and [32], the author has addressed the issues of clock offset and propagation speed estimation separately. The main contribution of this paper is the design and analysis of a novel navigation filter that unifies both concepts. In short, a OWTT navigation setting is assumed but the clock of the receiver installed on-board does not need to be synchronized with those of the emitters. Additionally, the speed of propagation of the acoustic waves in the medium is also unknown. A filtering solution is proposed, effectively bringing together the concepts introduced in [31] and [32], that yields estimates of the inertial position, inertial ocean current, clock offset, and speed of propagation of the acoustic waves. This setting potentially reduces the required hardware and simplifies deployment, as the clock of the vehicle does not need to be synchronized and the speed of sound does not need to be profiled. The discrete-time nature of the pseudo-range measurements is taken into account, the observability of the system is carefully analyzed, and the errors of the estimates, provided by a Kalman filter, converge exponentially fast to zero for all initial conditions. Higher rate attitude and velocity measurements drive the system dynamics between pseudo-range measurement updates. Initial work was presented in [33], where the novel problem framework was first introduced and the overall system dynamics proposed. This paper presents a unified and thorough presentation and analysis of the solution and it includes all the theorems and proofs that had been omitted in the conference paper. It also includes additional theoretical results, the discussion of several issues, and an additional solution without state augmentation. Finally, extensive and realistic simulations are also presented in detail, including cases with slowly time-varying quantities. The performance is evaluated also with Monte Carlo runs and the comparison with the EKF and the Bayesian Cramér-Rao bound is also included.

The paper is organized as follows. The problem statement and the nominal system dynamics are introduced in Section 2. The proposed filter design is detailed in Section 3, including a thorough observability analysis and the discussion of multi-rate implementations. Extensive simulation results are presented in Section 4, including the comparison with the EKF and the Bayesian Cramér-Rao bound (BRCB), and Section 5 summarizes the main results of the paper.

1.1. Notation

Throughout the paper, the symbol $\mathbf{0}_{n\times m}$ denotes a $n \times m$ matrix of zeros and $\mathbf{I}_n$ an identity matrix of dimensions $n \times n$. A square matrix of zeros of dimension $n \times n$ is simply represented by $\mathbf{0}_n$. A block diagonal matrix is represented by $\mathbf{diag}(\mathbf{A}_1, \ldots, \mathbf{A}_n)$. For $\mathbf{x} \in \mathbb{R}^3$ and $\mathbf{y} \in \mathbb{R}^3$, $\mathbf{x} \cdot \mathbf{y}$ and $\mathbf{x} \times \mathbf{y}$ represent the inner and cross products, respectively. The Special Orthogonal Group is denoted by $SO(3) := \left\{\mathbf{X} \in \mathbb{R}^{3\times3} : \mathbf{X}\mathbf{X}^T = \mathbf{X}^T\mathbf{X} = \mathbf{I}_3 \wedge \det(\mathbf{X}) = 1\right\}$. For convenience, define also the transpose operator $(.)^T$, and notice that $\mathbf{x} \cdot \mathbf{y} = \mathbf{x}^T\mathbf{y}$, $\mathbf{x}, \mathbf{y} \in \mathbb{R}^3$.

2. Problem statement

Consider a scenario where a set of acoustic emitters are installed in an LBL configuration and an underwater vehicle, equipped with an acoustic receiver, operates. The emitters are fixed, their clocks are synchronized and their inertial positions are available to the vehicle. Periodically, the emitters send acoustic signals, which are received by the vehicle. Additionally, the vehicle is also equipped with a Doppler velocity log

(DVL) and an attitude and heading reference system (AHRS). In a typical OWTT-LBL positioning system, the clocks of the emitters and the vehicle are synchronized, time tags are sent along the acoustic signals, and the speed of propagation of the waves is known, so that the vehicle can determine directly the distance to each emitter. Two key differences are considered in this paper: i) the speed of propagation of the waves is not known; and ii) the clock of the vehicle is not necessarily synchronized with those of the emitters. The problem addressed in this paper is that of designing a continuous-discrete filter, with globally exponentially stable error dynamics, to estimate the inertial position and velocity of the vehicle, as well as the offset between the emitting and receiving clocks and the speed of propagation of the acoustic waves in the medium.

2.1. System dynamics

Denote by $\{\mathcal{I}\}$ a local inertial coordinate frame and by $\{\mathcal{B}\}$ a coordinate frame attached to the vehicle, usually referred to as the body-fixed reference frame. The linear motion of the vehicle satisfies

$$\dot{\mathbf{p}}(t) = \mathbf{R}(t)\mathbf{v}(t), \tag{1}$$

where $\mathbf{p}(t) \in \mathbb{R}^3$ corresponds to its inertial position, $\mathbf{v}(t) \in \mathbb{R}^3$ is the velocity of the vehicle relative to $\{\mathcal{I}\}$, expressed in $\{\mathcal{B}\}$, and $\mathbf{R}(t) \in SO(3)$ is the rotation matrix from $\{\mathcal{B}\}$ to $\{\mathcal{I}\}$.

The attitude of the vehicle, described by $\mathbf{R}(t)$, is provided by the AHRS, whereas the DVL measures, in the absence of bottom-lock, the velocity of the vehicle relative to the fluid, expressed in body-fixed coordinates. Denote by $\mathbf{v}_c(t) \in \mathbb{R}^3$ the velocity of the fluid, in inertial coordinates, and by $\mathbf{v}_r(t) \in \mathbb{R}^3$ the DVL reading, i.e., the velocity of the vehicle relative to the fluid, expressed in body-fixed coordinates. Then, the inertial velocity of the vehicle, expressed in body-fixed coordinates, satisfies

$$\mathbf{v}(t) = \mathbf{R}^T(t)\mathbf{v}_c(t) + \mathbf{v}_r(t). \tag{2}$$

Finally, denote by $\mathbf{s}_i \in \mathbb{R}^3$, $i = 1, \ldots, L$, the inertial positions of the acoustic emitters. Then, the pseudo-range measurements can be written as

$$r_i(k) = v_s(t_k)\,\|\mathbf{s}_i - \mathbf{p}(t_k)\| + b_c(t_k), \tag{3}$$

with $t_k := t_0 + kT$, $k \in \mathbb{N}$, where $T > 0$ is the sampling period, t_0 is the initial time, $b_c(t_k)$ is a bias term that accounts for the effect of the offset between the emitting and receiving clocks, and $v_s(t_k)$ is the term that accounts for the unknown speed of propagation of the acoustic waves in the medium. Notice that $v_s(t_k)$ is not the speed of propagation of the acoustic waves in the medium. Instead, it is an unknown dimensionless scaling factor that corresponds to the ratio between the nominal speed that is assumed by the range sensor and the actual unknown speed of propagation of the acoustic waves in the medium. Likewise, $b_c(t_k)$ is not the actual clock offset. Instead, it corresponds to the distance offset that results from the clock offset at the nominal speed of propagation of the acoustic waves in the medium that is assumed by the acoustic positioning system.

The following assumptions are considered in the paper.

Assumption 1. *The pseudo-range measurements are positive, i.e., $r_i(k) > 0$ for all k and $i = 1, \ldots, L$.*

Assumption 2. *The inertial fluid velocity is constant, i.e., $\dot{\mathbf{v}}_c(t) = \mathbf{0}_{3\times1}$.*

Assumption 3. *Both the nominal speed that is assumed by the range sensor and the actual speed of propagation of the acoustic waves in the medium are constant, hence $\dot{v}_s(t) = 0$.*

Assumption 4. *The offset of the clocks is constant, hence $\dot{b}_c(t) = 0$.*

The technical condition stated in Assumption 1 is a mild one, which can always be verified in practice. Indeed, if the time tag of a signal received by the vehicle was greater than the clock of the receiver, the receiver would immediately know that its clock is behind and could reset it to a higher value, so that the pseudo-range measurement is positive. The remaining three assumptions are standard [7, 9] and they are required for system modeling purposes. In practice, the solution that is proposed in the paper can be tuned to track slowly time-varying quantities. This will be detailed later on.

Combining (1)-(3) and considering Assumptions 2 to 4 gives the nonlinear system with discrete outputs

$$\begin{cases} \dot{\mathbf{p}}(t) = \mathbf{v}_c(t) + \mathbf{R}(t)\mathbf{v}_r(t) \\ \dot{\mathbf{v}}_c(t) = \mathbf{0}_{3\times1} \\ \dot{v}_s(t) = 0 \\ \dot{b}_c(t) = 0 \\ r_1(k) = v_s(t_k)\,\|\mathbf{s}_1 - \mathbf{p}(t_k)\| + b_c(t_k) \\ \vdots \\ r_L(k) = v_s(t_k)\,\|\mathbf{s}_L - \mathbf{p}(t_k)\| + b_c(t_k) \end{cases}. \tag{4}$$

The problem considered in this paper is the design of an estimator for (4) with globally exponentially stable error dynamics.

3. Filter design

The two main issues regarding LBL navigation that are addressed simultaneously in this paper, namely i) dealing with unknown speeds of propagation of the acoustic waves in the medium; and ii) dealing with unknown clock offsets between the emitters and the receivers have been addressed separately in the past. In particular, the latter was considered in [31], where a novel long baseline navigation solution was proposed considering that there is an unknown clock offset between the acoustic emitters and the receiver. In that work, discrete-time pseudo-range measurements were considered, the system dynamics were augmented with the pseudo-range differences and the LBL geometry was also encoded through an augmented output in such a way that the resulting system dynamics could be considered as linear. The former was considered in [32], where the state was redefined considering scaled position and linear velocity states, augmenting also the state with the pseudo-range measurements, and considering also an augmented output to encode the LBL geometry of the problem, in such a way that the

resulting system, although nonlinear, could be treated resorting to linear systems theory. This paper brings together these different concepts.

The original system dynamics (4) has a continuous-discrete nature, in the sense that the dynamics evolve in continuous time but the measurements that can be used to close the loop and force the estimation error to converge to zero are only available in discrete-time. In Section 3.1 a discrete-time system is presented and an augmented system is derived that captures all the essential properties of the original system dynamics. The observability of that system is analyzed in Section 3.2, whereas the final estimation solution is proposed in Section 3.3, taking into account the existence of sensor measurements that are acquired at high rates and that can be used to drive the estimates between update instants. An alternative simpler solution, without state augmentation, is briefly presented in Section 3.4.

3.1. Discretization and system augmentation

The exact discrete-time system dynamics corresponding to (4) are given by

$$\begin{cases} \mathbf{p}\left(t_{k+1}\right) = \mathbf{p}\left(t_k\right) + T\mathbf{v}_c\left(t_k\right) + \int_{t_k}^{t_{k+1}} \mathbf{R}\left(\tau\right)\mathbf{v}_r\left(\tau\right)d\tau \\ \mathbf{v}_c\left(t_{k+1}\right) = \mathbf{v}_c\left(t_k\right) \\ v_s\left(t_{k+1}\right) = v_s\left(t_k\right) \\ b_c\left(t_{k+1}\right) = b_c\left(t_k\right) \\ r_1\left(k\right) = v_s\left(t_k\right)\left\|\mathbf{s}_1 - \mathbf{p}\left(t_k\right)\right\| + b_c\left(t_k\right) \\ \vdots \\ r_L\left(k\right) = v_s\left(t_k\right)\left\|\mathbf{s}_L - \mathbf{p}\left(t_k\right)\right\| + b_c\left(t_k\right) \end{cases}. \tag{5}$$

In a similar fashion to [31], but considering also the clock offset, define the discrete-time states

$$\begin{cases} \mathbf{x}_1(k) := v_s^2\left(t_k\right)\mathbf{p}\left(t_k\right) \\ \mathbf{x}_2(k) := v_s^2\left(t_k\right)\mathbf{v}_c\left(t_k\right) \\ x_3\left(k\right) := v_s^2\left(t_k\right) \\ x_4\left(k\right) = b_c\left(t_k\right) \end{cases}, \tag{6}$$

which correspond to a scaled inertial position of the vehicle, a scaled inertial current velocity, and factors that account for the clock offset and the speed of propagation of the acoustic signals in the medium. From (5) one may write

$$\begin{cases} \mathbf{x}_1\left(k+1\right) = \mathbf{x}_1\left(k\right) + T\mathbf{x}_2\left(k\right) + x_3\left(k\right)\mathbf{u}\left(k\right) \\ \mathbf{x}_2\left(k+1\right) = \mathbf{x}_2\left(k\right) \\ x_3\left(k+1\right) = x_3\left(k\right) \\ x_4\left(k+1\right) = x_4\left(k\right) \end{cases}, \tag{7}$$

with $\mathbf{u}(k) := \int_{t_k}^{t_{k+1}} \mathbf{R}\left(\tau\right)\mathbf{v}_r\left(\tau\right)d\tau$.

Next, equations that encode the LBL structure of the problem are derived. To that purpose, rearrange (3) as

$$r_i(k) - b_c\left(t_k\right) = v_s\left(t_k\right)\left\|\mathbf{s}_i - \mathbf{p}\left(t_k\right)\right\|,\ i = 1, \ldots, L. \tag{8}$$

Taking the squares of both sides of (8), considering the state definition (6), and taking the difference for different pairs of emitters allows to write

$$\begin{aligned} &\left[r_i(k) - b_c\left(t_k\right)\right]^2 - \left[r_j(k) - b_c\left(t_k\right)\right]^2 = \\ &r_i^2\left(k\right) - r_j^2\left(k\right) - 2\left[r_i\left(k\right) - r_j\left(k\right)\right]x_4\left(k\right) \end{aligned} \tag{9}$$

and

$$\begin{aligned} &\left[r_i(k) - b_c\left(t_k\right)\right]^2 - \left[r_j(k) - b_c\left(t_k\right)\right]^2 = \\ &-2\left(\mathbf{s}_i - \mathbf{s}_j\right)\cdot\mathbf{x}_1(k) + \left(\left\|\mathbf{s}_i\right\|^2 - \left\|\mathbf{s}_j\right\|^2\right)x_3(k) \end{aligned} \tag{10}$$

for all $i,\ j \in \{1, \ldots, L\}$, $i \neq j$. Comparing (9) with (10) allows to further write

$$\begin{aligned} r_i^2\left(k\right) - r_j^2\left(k\right) &= -2\left(\mathbf{s}_i - \mathbf{s}_j\right)\cdot\mathbf{x}_1(k) \\ &+ \left(\left\|\mathbf{s}_i\right\|^2 - \left\|\mathbf{s}_j\right\|^2\right)x_3(k) + 2\left[r_i\left(k\right) - r_j\left(k\right)\right]x_4\left(k\right) \end{aligned} \tag{11}$$

for all $i,\ j \in \{1, \ldots, L\}$, $i \neq j$, or, equivalently,

$$\begin{aligned} &2\tfrac{\mathbf{s}_i - \mathbf{s}_j}{r_i(k) + r_j(k)}\cdot\mathbf{x}_1(k) - \tfrac{\left\|\mathbf{s}_i\right\|^2 - \left\|\mathbf{s}_j\right\|^2}{r_i(k) + r_j(k)}x_3(k) \\ &-2\tfrac{r_i(k) - r_j(k)}{r_i(k) + r_j(k)}x_4(k) + \left[r_i(k) - r_j(k)\right] = 0 \end{aligned} \tag{12}$$

for all $i,\ j \in \{1, \ldots, L\}$, $i \neq j$. Notice that (12) effectively encodes the LBL structure of the problem. This derivation bears resemblance with those presented in [31], [32], and [34]. However, in [34], neither the clock offset nor the speed of propagation of the acoustic signals were considered; in [31] the speed of propagation of the acoustic signals is considered but not the clock offset; in [32] the clock offset is considered but not the speed of propagation of the acoustic signals.

As it is interesting in terms of filtering performance, the differences between the pseudo-range measurements are also included in the system state. Define these new states as

$$\begin{cases} x_5(k) = r_1(k) - r_2(k) \\ x_6(k) = r_1(k) - r_3(k) \\ \vdots \\ x_{3+C_2^L}(k) = r_{L-2}(k) - r_L(k) \\ x_{4+C_2^L}(k) = r_{L-1}(k) - r_L(k) \end{cases},$$

where C_2^L is the number of 2-combinations of L elements, i.e., $C_2^L = L\left(L-1\right)/2$. It is a matter of computation (see Appendix A) to show that the dynamics of the new states can be written as

$$\begin{aligned} r_i\left(k+1\right) - r_j\left(k+1\right) &= -2T\tfrac{\mathbf{s}_i - \mathbf{s}_j}{r_i(k+1) + r_j(k+1)}\cdot\mathbf{x}_2(k) \\ &-2\tfrac{\left(\mathbf{s}_i - \mathbf{s}_j\right)\cdot\mathbf{u}(k)}{r_i(k+1) + r_j(k+1)}x_3(k) \\ &+2\tfrac{\left[r_i(k+1) - r_i(k)\right] - \left[r_j(k+1) - r_j(k)\right]}{r_i(k+1) + r_j(k+1)}x_4(k) \\ &+\tfrac{r_i(k) + r_j(k)}{r_i(k+1) + r_j(k+1)}\left[r_i\left(k\right) - r_j(k)\right] \end{aligned} \tag{13}$$

for all $i,\ j \in \{1, \ldots, L\}$, $i \neq j$.

Next, the augmented system will be introduced in compact form. Before that, in order to simplify the notation and for the sake of clarity of presentation, define

$$\mathbf{M}_1 := \begin{bmatrix} \left(\mathbf{s}_1 - \mathbf{s}_2\right)^T \\ \left(\mathbf{s}_1 - \mathbf{s}_3\right)^T \\ \vdots \\ \left(\mathbf{s}_{L-2} - \mathbf{s}_L\right)^T \\ \left(\mathbf{s}_{L-1} - \mathbf{s}_L\right)^T \end{bmatrix} \in \mathbb{R}^{C_2^L \times 3},$$

$$\mathbf{M}_2 := \begin{bmatrix} \|\mathbf{s}_1\|^2 - \|\mathbf{s}_2\|^2 \\ \|\mathbf{s}_1\|^2 - \|\mathbf{s}_3\|^2 \\ \vdots \\ \|\mathbf{s}_{L-2}\|^2 - \|\mathbf{s}_L\|^2 \\ \|\mathbf{s}_{L-1}\|^2 - \|\mathbf{s}_L\|^2 \end{bmatrix} \in \mathbb{R}^{C_2^L},$$

$$\mathbf{D}(k) := \begin{bmatrix} r_1(k) - r_2(k) \\ r_1(k) - r_3(k) \\ \vdots \\ r_{L-2}(k) - r_L(k) \\ r_{L-1}(k) - r_L(k) \end{bmatrix} \in \mathbb{R}^{C_2^L},$$

and

$$\mathbf{E}(k) := \mathbf{diag}\left(r_1(k) + r_2(k), r_1(k) + r_3(k), \ldots, r_{L-2}(k) + r_L(k), r_{L-1}(k) + r_L(k)\right) \in \mathbb{R}^{C_2^L \times C_2^L}.$$

Define the augmented state vector as

$$\mathbf{x}(k) := \begin{bmatrix} \mathbf{x}_1(k) \\ \mathbf{x}_2(k) \\ x_3(k) \\ x_4(k) \\ x_5(k) \\ \vdots \\ x_{4+C_2^L}(k) \end{bmatrix} \in \mathbb{R}^{3+3+2+C_2^L}.$$

Then, collecting (7) and (13), it is possible to write the discrete-time state equation as

$$\mathbf{x}(k+1) = \mathbf{A}(k)\mathbf{x}(k), \tag{14}$$

where $\mathbf{A}(k) \in \mathbb{R}^{(8+C_2^L)\times(8+C_2^L)}$,

$$\mathbf{A}(k) = \left[\begin{array}{cccc|c} \mathbf{I}_3 & T\mathbf{I}_3 & \mathbf{u}(k) & \mathbf{0}_{3\times 1} & \mathbf{0}_{3\times C_2^L} \\ \mathbf{0}_3 & \mathbf{I}_3 & \mathbf{0}_{3\times 1} & \mathbf{0}_{3\times 1} & \mathbf{0}_{3\times C_2^L} \\ \mathbf{0}_{1\times 3} & \mathbf{0}_{1\times 3} & 1 & 0 & \mathbf{0}_{1\times C_2^L} \\ \mathbf{0}_{1\times 3} & \mathbf{0}_{1\times 3} & 0 & 1 & \mathbf{0}_{1\times C_2^L} \\ \hline \mathbf{0}_{C_2^L\times 3} & \mathbf{A}_{52}(k) & \mathbf{A}_{53}(k) & \mathbf{A}_{54}(k) & \mathbf{A}_{55}(k) \end{array}\right],$$

with

$$\mathbf{A}_{52}(k) = -2T\mathbf{E}^{-1}(k+1)\mathbf{M}_1 \in \mathbb{R}^{C_2^L\times 3},$$

$$\mathbf{A}_{53}(k) = -2\mathbf{E}^{-1}(k+1)\mathbf{M}_1\mathbf{u}(k) \in \mathbb{R}^{C_2^L},$$

$$\mathbf{A}_{54}(k) = 2\mathbf{E}^{-1}(k+1)\left(\mathbf{D}(k+1) - \mathbf{D}(k)\right) \in \mathbb{R}^{C_2^L},$$

and

$$\mathbf{A}_{55}(k) = \mathbf{E}^{-1}(k+1)\mathbf{E}(k) \in \mathbb{R}^{C_2^L\times C_2^L}.$$

In order to derive the complete augmented system, an output must be considered in addition to the dynamics (14). To that purpose, ignore for now the original nonlinear output (3) and consider instead (12). Furthermore, notice that the states $x_5(k), \ldots, x_{4+C_2^L}(k)$ are available from the pseudo-range measurements, which allows to write, in compact form,

$$\begin{cases} \mathbf{x}(k+1) = \mathbf{A}(k)\mathbf{x}(k) \\ \mathbf{y}(k) = \mathbf{C}(k)\mathbf{x}(k) \end{cases}, \tag{15}$$

with $\mathbf{C}(k) \in \mathbb{R}^{2C_2^L\times(8+C_2^L)}$,

$$\mathbf{C}(k) = \begin{bmatrix} \mathbf{0}_{C_2^L\times 3} & \mathbf{0}_{C_2^L\times 3} & \mathbf{0}_{C_2^L\times 1} & \mathbf{0}_{C_2^L\times 1} & \mathbf{I}_{C_2^L} \\ \mathbf{C}_{21}(k) & \mathbf{0}_{C_2^L\times 3} & \mathbf{C}_{23}(k) & \mathbf{C}_{24}(k) & \mathbf{I}_{C_2^L} \end{bmatrix},$$

$$\mathbf{C}_{21}(k) = 2\mathbf{E}^{-1}(k)\mathbf{M}_1 \in \mathbb{R}^{C_2^L\times 3},$$

$$\mathbf{C}_{23}(k) = -\mathbf{E}^{-1}(k)\mathbf{M}_2 \in \mathbb{R}^{C_2^L},$$

and

$$\mathbf{C}_{24}(k) = -2\mathbf{E}^{-1}\mathbf{D}(k) \in \mathbb{R}^{C_2^L}.$$

In short, in addition to the dynamics (14), two groups of outputs are considered: i) the first C_2^L rows of $\mathbf{C}(k)$ encode the fact that the pseudo-range differences are available and, for this augmented system, are a linear function of its state; and ii) the last C_2^L rows of $\mathbf{C}(k)$ encode (12), which effectively describes the LBL structure, through the appropriate defintion of $\mathbf{C}_{21}(k)$, $\mathbf{C}_{23}(k)$, and $\mathbf{C}_{24}(k)$.

Notice that the system (15) is well defined under Assumption 1. Moreover, the system matrix $\mathbf{A}(k)$ is invertible for all time since its determinant corresponds to the product of its diagonal elements, which is the product of the diagonal terms of $\mathbf{A}_{55}(k)$, all positive under Assumption 1.

3.2. Observability analysis

The discrete time-varying system (15) can be regarded as linear in the state for observer design purposes, even though the system matrices $\mathbf{A}(k)$ and $\mathbf{C}(k)$ depend on the pseudo-range measurements, as well as on the input $\mathbf{u}(k)$. This is possible because both the input and the pseudo-range measurements are available. Hence, they can be simply considered as functions of time. Therefore, linear system theory applies.

The following theorem addresses the observability of (15).

Theorem 1. *Let k_0 denote the initial discrete-time instant. Define, for $k_i \geq k_0$,*

$$\mathbf{L}(k_i) := \begin{bmatrix} \mathbf{L}_1 & \mathbf{L}_2 & \mathbf{L}_3(k_i) \end{bmatrix} \in \mathbb{R}^{C_2^L\times 5},$$

with $\mathbf{L}_1 := 2\mathbf{M}_1$, $\mathbf{L}_2 := -\mathbf{M}_2$, and $\mathbf{L}_3(k_i) := -2\mathbf{D}(k)$. Suppose that the configuration of the LBL acoustic positioning system is such that $\mathbf{L}(k_i)$ is full rank, i.e.,

$$\mathrm{rank}\left(\mathbf{L}(\mathrm{k_i})\right) = 5, \tag{16}$$

Then, the discrete-time system (15) *is observable on the interval $[k_i, k_i + 2]$, in the sense that the initial state $\mathbf{x}(k_i)$ is uniquely determined by the input $\{\mathbf{u}(k) : k = k_i, k_i + 1\}$ and the output $\{\mathbf{y}(k) : k = k_i, k_i + 1\}$.*

Proof. First, notice that if the rank of the observability matrix $\boldsymbol{O}(k_i, k_i + 2)$ associated with the pair $(\mathbf{A}(k), \mathbf{C}(k))$ on $[k_i, k_i + 2]$, $k_i \geq k_0$, is equal to the number of states of the system, then the system is observable. The proof follows by contradiction. Fix $k_i \geq k_0$, suppose that (16) holds and the system is not observable. Then, there exists a unit vector $\mathbf{d} = \begin{bmatrix} \mathbf{d}_1^T & \mathbf{d}_2^T & d_3 & d_4 & \mathbf{d}_5^T \end{bmatrix}^T \in \mathbb{R}^{3+3+1+1+C_2^L}$, with $\mathbf{d}_1, \mathbf{d}_2 \in \mathbb{R}^3$,

$d_3, d_4 \in \mathbb{R}$, $\mathbf{d}_5 \in \mathbb{R}^{C_2^L}$, such that $\boldsymbol{O}(k_i, k_i+2)\,\mathbf{d} = \mathbf{0}_{4C_2^L\times 1}$ or, equivalently,

$$\begin{cases} \mathbf{C}(k_i)\,\mathbf{d} = \mathbf{0}_{2C_2^L\times 1} \\ \mathbf{C}(k_i+1)\,\mathbf{A}(k_i)\,\mathbf{d} = \mathbf{0}_{2C_2^L\times 1} \end{cases}. \tag{17}$$

From the first equation of (17), and attending to the structure of $\mathbf{C}(k_i)$, in particular to the upper part of $\mathbf{C}(k_i)$, one immediately concludes that $\mathbf{d}_5 = \mathbf{0}_{C_2^L\times 1}$. Substituting that in the first equation of (17) but considering now the lower part of $\mathbf{C}(k_i)$ allows to write $\mathbf{C}_{21}(k_i)\,\mathbf{d}_1 + \mathbf{C}_{23}(k_i)\,\mathbf{d}_3 + \mathbf{C}_{24}(k_i)\,\mathbf{d}_4 = \mathbf{0}_{C_2^L\times 1}$ or, equivalently,

$$\mathbf{E}^{-1}(k_i)\,\mathbf{L}(k_i)\begin{bmatrix}\mathbf{d}_1\\ d_3\\ d_4\end{bmatrix} = \mathbf{0}_{C_2^L\times 1}. \tag{18}$$

Since (16) is assumed to hold, then the only solution of (18) is $\mathbf{d}_1 = \mathbf{0}_{3\times 1}$, $d_3 = 0$, and $d_4 = 0$. Now, with that in mind, as well as $\mathbf{d}_5 = \mathbf{0}_{C_2^L\times 1}$, one may write, from the second equation of (17), that $\mathbf{A}_{52}(k_i)\,\mathbf{d}_2 = \mathbf{0}_{C_2^L\times 1}$ or, equivalently,

$$-T\mathbf{E}^{-1}(k_i+1)\,\mathbf{L}_1\mathbf{d}_2. \tag{19}$$

Moreover, as $\mathbf{d}$ is a unit vector and all the other components but $\mathbf{d}_2$ were shown to be null, it follows that $\mathbf{d}_2$ must be a unit vector. Moreover, it is possible to write, from (19), that

$$\mathbf{L}(k_i)\begin{bmatrix}\mathbf{d}_2\\ 0\\ 0\end{bmatrix} = \mathbf{0}_{C_2^L},$$

which implies that $\mathbf{L}(k_i)$ is not full rank. But that contradicts the hypothesis (16), thus concluding the proof. □

When the augmented system (15) was derived, some nonlinear constraints were disregarded to attain linear dynamics. As a result, it is now important to establish that the augmented system (15) does indeed relate to the original nonlinear system (5). This is the subject of the following theorem.

Theorem 2. *Suppose that* (16) *holds for some* $k_i \geq k_0$. *Then:*

i) the nonlinear system (5) *is observable on the interval* $[k_i, k_i+2]$ *in the sense that the initial state* $\mathbf{x}(k_i)$ *is uniquely determined by the input* $\{\mathbf{u}(k) : k = k_i, k_i+1\}$ *and the output* $\{r_1(k), \ldots, r_L(k) : k = k_i, k_i+1\}$*; and*

ii) the initial condition of the augmented system (15) *corresponds to that of* (5) *on the interval* $[k_i, k_i+2]$*, i.e.,*

$$\begin{cases} \mathbf{x}_1(k_i) = v_s^2(t_{k_i})\,\mathbf{p}(t_{k_i}) \\ \mathbf{x}_2(k_i) = v_s^2(t_{k_i})\,\mathbf{v}_c(t_{k_i}) \\ x_3(k_i) = v_s^2(t_{k_i}) \\ x_4(k_i) = b_c(t_{k_i}) \\ x_5(k_i) = v_s(t_{k_i})\left[\left\|\mathbf{s}_1 - \mathbf{p}(t_{k_i})\right\| - \left\|\mathbf{s}_2 - \mathbf{p}(t_{k_i})\right\|\right] \\ x_6(k_i) = v_s(t_{k_i})\left[\left\|\mathbf{s}_1 - \mathbf{p}(t_{k_i})\right\| - \left\|\mathbf{s}_3 - \mathbf{p}(t_{k_i})\right\|\right] \\ \vdots \\ x_{3+C_2^L}(k_i) = v_s(t_{k_i})\left[\left\|\mathbf{s}_{L-2} - \mathbf{p}(t_{k_i})\right\| - \left\|\mathbf{s}_L - \mathbf{p}(t_{k_i})\right\|\right] \\ x_{4+C_2^L}(k_i) = v_s(t_{k_i})\left[\left\|\mathbf{s}_{L-1} - \mathbf{p}(t_{k_i})\right\| - \left\|\mathbf{s}_L - \mathbf{p}(t_{k_i})\right\|\right] \end{cases}.$$

Proof. In order to prove ii), the outputs of both systems are compared and it is shown that the initial conditions must match under the conditions of the theorem. The proof of i) follows directly from this since the initial condition of the linear system is uniquely determined, and hence so must be the initial condition of the nonlinear system. Let

$$\mathbf{x}(k_i) := \begin{bmatrix} \mathbf{x}_1(k_i) \\ \mathbf{x}_2(k_i) \\ x_3(k_i) \\ x_4(k_i) \\ x_5(k_i) \\ \vdots \\ x_{4+C_2^L}(k_i) \end{bmatrix} \in \mathbb{R}^{3+3+1+1+C_2^L}$$

denote the initial condition of (15) and let $\mathbf{p}(t_{k_i})$, $\mathbf{v}_c(t_{k_i})$, $v_s(t_{k_i})$, and $b_c(t_{k_i})$ be the initial condition of (5). From the first C_2^L outputs of (15) it must be

$$\begin{cases} x_5(k_i) = r_1(k_i) - r_2(k_i) \\ x_6(k_i) = r_1(k_i) - r_3(k_i) \\ \vdots \\ x_{3+C_2^L}(k_i) = r_{L-2}(k_i) - r_L(k_i) \\ x_{4+C_2^L}(k_i) = r_{L-1}(k_i) - r_L(k_i) \end{cases} \tag{20}$$

or, equivalently,

$$\begin{cases} x_5(k_i) = v_s(t_{k_i})\left[\left\|\mathbf{s}_1 - \mathbf{p}(t_{k_i})\right\| - \left\|\mathbf{s}_2 - \mathbf{p}(t_{k_i})\right\|\right] \\ x_6(k_i) = v_s(t_{k_i})\left[\left\|\mathbf{s}_1 - \mathbf{p}(t_{k_i})\right\| - \left\|\mathbf{s}_3 - \mathbf{p}(t_{k_i})\right\|\right] \\ \vdots \\ x_{3+C_2^L}(k_i) = v_s(t_{k_i})\left[\left\|\mathbf{s}_{L-2} - \mathbf{p}(t_{k_i})\right\| - \left\|\mathbf{s}_L - \mathbf{p}(t_{k_i})\right\|\right] \\ x_{4+C_2^L}(k_i) = v_s(t_{k_i})\left[\left\|\mathbf{s}_{L-1} - \mathbf{p}(t_{k_i})\right\| - \left\|\mathbf{s}_L - \mathbf{p}(t_{k_i})\right\|\right] \end{cases}.$$

Consider now the differences of pseudo-range measurements of the nonlinear system (5) for $k = k_i$ as a function of its initial state, which can be written as

$$\begin{aligned} r_l(k_i) - r_m(k_i) &= -2\tfrac{\mathbf{s}_l - \mathbf{s}_m}{r_l(k_i)+r_m(k_i)} \cdot v_s^2(t_{k_i})\,\mathbf{p}(t_{k_i}) \\ &+ \tfrac{\|\mathbf{s}_l\|^2 - \|\mathbf{s}_m\|^2}{r_l(k_i)+r_m(k_i)} v_s^2(t_{k_i}) + 2\tfrac{r_l(k_i)-r_m(k_i)}{r_l(k_i)+r_m(k_i)} b_c(t_{k_i}) \end{aligned} \tag{21}$$

for all $l, m \in \{1, \ldots, L\}$, $l \neq m$. On the other hand, evaluating the outputs of (15) $y_{C_2^L+1}(k)$ to $y_{2C_2^L}(k)$ for $k = k_i$ as a function of $\mathbf{x}(k_i)$, and considering (20), gives

$$\begin{aligned} r_l(k_i) - r_m(k_i) &= -2\tfrac{\mathbf{s}_l - \mathbf{s}_m}{r_l(k_i)+r_m(k_i)} \cdot \mathbf{x}_1(k_i) \\ &+ \tfrac{\|\mathbf{s}_l\|^2 - \|\mathbf{s}_m\|^2}{r_l(k_i)+r_m(k_i)} x_3(k_i) + 2\tfrac{r_l(k_i)-r_m(k_i)}{r_l(k_i)+r_m(k_i)} x_4(k_i) \end{aligned} \tag{22}$$

for all $l, m \in \{1, \ldots, L\}$, $l \neq m$. Comparing (21) with (22) allows to write

$$\begin{aligned} &2\tfrac{\mathbf{s}_l - \mathbf{s}_m}{r_l(k_i)+r_m(k_i)} \cdot \left[v_s^2(t_{k_i})\,\mathbf{p}(t_{k_i}) - \mathbf{x}_1(k_i)\right] \\ &\quad - \tfrac{\|\mathbf{s}_l\|^2 - \|\mathbf{s}_m\|^2}{r_l(k_i)+r_m(k_i)}\left[v_s^2(t_{k_i}) - x_3(k_i)\right] \\ &\quad -2\tfrac{r_l(k_i)-r_m(k_i)}{r_l(k_i)+r_m(k_i)}\left[b_c(t_{k_i}) - x_4(k_i)\right] = 0 \end{aligned}$$

for all l, $m \in \{1, \ldots, L\}$, $l \neq m$, or, in compact form,

$$\mathbf{L}(k_i)\begin{bmatrix} v_s^2(t_{k_i})\,\mathbf{p}(t_{k_i}) - \mathbf{x}_1(k_i) \\ v_s^2(t_{k_i}) - x_3(k_i) \\ b_c(t_{k_i}) - x_4(k_i) \end{bmatrix} = \mathbf{0}_{C_2^L \times 1}. \tag{23}$$

If (16) holds, the only solution of (23) is

$$\begin{cases} \mathbf{x}_1(k_i) = v_s^2(t_{k_i})\,\mathbf{p}(t_{k_i}) \\ x_3(k_i) = v_s^2(t_{k_i}) \\ x_4(k_i) = b_c(t_{k_i}) \end{cases}. \tag{24}$$

Now, for $k = k_i + 1$ it is possible to write the differences of pseudo-ranges as a function of the initial state of (5) as

$$\begin{aligned} r_l(k_i+1) - r_m(k_i+1) = v_s^2\left(t_{k_i}\right)\tfrac{\|\mathbf{s}_l\|^2 - \|\mathbf{s}_m\|^2}{r_l(k_i+1)+r_m(k_i+1)} \\ -2v_s^2\left(t_{k_i}\right)\tfrac{\mathbf{s}_l-\mathbf{s}_m}{r_l(k_i+1)+r_m(k_i+1)}\cdot\left[\mathbf{p}\left(t_{k_i}\right) + T\mathbf{v}_c\left(t_{k_i}\right) + \mathbf{u}(k_i)\right] \\ +2\tfrac{r_l(k_i+1)-r_m(k_i+1)}{r_l(k_i+1)+r_m(k_i+1)}b_c\left(t_{k_i}\right) \end{aligned} \tag{25}$$

for all l, $m \in \{1, \ldots, L\}$, $l \neq m$. From the first C_2^L outputs of (15) for $k = k_i + 1$ it follows that

$$\begin{aligned} r_l(k_i+1) - r_m(k_i+1) = &-2T\tfrac{\mathbf{s}_l-\mathbf{s}_m}{r_l(k_i+1)+r_m(k_i+1)}\cdot\mathbf{x}_2(k_i) \\ &-2\tfrac{\mathbf{s}_l-\mathbf{s}_m}{r_l(k_i+1)+r_m(k_i+1)}\cdot\mathbf{u}(k_i)\,x_3(k_i) \\ &+2\tfrac{r_l(k_i+1)-r_m(k_i+1)}{r_l(k_i+1)+r_m(k_i+1)}x_4(k_i) - 2\tfrac{r_l(k_i)-r_m(k_i)}{r_l(k_i+1)+r_m(k_i+1)}x_4(k_i) \\ &+\tfrac{r_l(k_i)+r_m(k_i)}{r_l(k_i+1)+r_m(k_i+1)}\left[x_{4+l}(k_i) - x_{4+m}(k_i)\right] \end{aligned}$$

for all l, $m \in \{1, \ldots, L\}$, $l \neq m$. Using (20) and (24), it is possible to further write

$$\begin{aligned} r_l(k_i+1) - r_m(k_i+1) = &-2T\tfrac{\mathbf{s}_l-\mathbf{s}_m}{r_l(k_i+1)+r_m(k_i+1)}\cdot\mathbf{x}_2(k_i) \\ &-2\tfrac{\mathbf{s}_l-\mathbf{s}_m}{r_l(k_i+1)+r_m(k_i+1)}\cdot\mathbf{u}(k_i)\,v_s^2(t_{k_i}) \\ &+2\tfrac{r_l(k_i+1)-r_m(k_i+1)}{r_l(k_i+1)+r_m(k_i+1)}b_c(t_{k_i}) - 2\tfrac{r_l(k_i)-r_m(k_i)}{r_l(k_i+1)+r_m(k_i+1)}b_c(t_{k_i}) \\ &+\tfrac{r_l(k_i)+r_m(k_i)}{r_l(k_i+1)+r_m(k_i+1)}\left[r_l(k_i) - r_m(k_i)\right] \end{aligned} \tag{26}$$

for all l, $m \in \{1, \ldots, L\}$, $l \neq m$. Substituting (22) in (26) and using (24) again gives

$$\begin{aligned} r_l(k_i+1) - r_m(k_i+1) = v_s^2(t_{k_i})\tfrac{\|\mathbf{s}_l\|^2 - \|\mathbf{s}_m\|^2}{r_l(k_i+1)+r_m(k_i+1)} \\ -2\tfrac{\mathbf{s}_l-\mathbf{s}_m}{r_l(k_i+1)+r_m(k_i+1)}\cdot v_s^2(t_{k_i})\,\mathbf{p}(t_{k_i}) \\ -2\tfrac{\mathbf{s}_l-\mathbf{s}_m}{r_l(k_i+1)+r_m(k_i+1)}\cdot T\mathbf{x}_2(k_i) \\ -2\tfrac{\mathbf{s}_l-\mathbf{s}_m}{r_l(k_i+1)+r_m(k_i+1)}\cdot v_s^2(t_{k_i})\,\mathbf{u}(k_i) \\ +2\tfrac{r_l(k_i+1)-r_m(k_i+1)}{r_l(k_i+1)+r_m(k_i+1)}b_c(t_{k_i}) \end{aligned} \tag{27}$$

for all l, $m \in \{1, \ldots, L\}$, $l \neq m$. Comparing (25) with (27) gives

$$2T\frac{\mathbf{s}_l - \mathbf{s}_m}{r_l(k_i+1) + r_m(k_i+1)}\cdot\left[\mathbf{x}_2(k_i) - v_s^2(t_{k_i})\,\mathbf{v}_c(t_{k_i})\right] = 0 \tag{28}$$

for all l, $m \in \{1, \ldots, L\}$, $l \neq m$. If (16) holds, then the only solution of (28) is

$$\mathbf{x}_2 = v_s^2(t_{k_i})\,\mathbf{v}_c(t_{k_i}).$$

This concludes the second part of the theorem, as it has been shown that, in the conditions of the theorem, the initial condition of (5) corresponds to that of (15). Now, notice that, using Theorem 1, the initial condition of (15) is uniquely determined. Since the two initial conditions match, it follows that the initial condition of (5) is also uniquely determined. □

The setup that was just presented is the most demanding one, where a vehicle estimates its inertial position and velocity based on pseudo-range measurements, estimating at the same time the clock offset between the vehicle and the emitters and the speed of propagation of the acoustic signals in the medium. In order for the rank condition (16) to be satisfied in general, at least 5 emitters are required. This number compares with 4 emitters for unique positioning with a long baseline system with synchronized clocks and known speed of propagation of the acoustic signals, see e.g. [27]. A simple way to decrease by one the number of emitters that are required is to consider an additional pressure/depth sensor, which gives the z-coordinate of the inertial position of the vehicle. In terms of the system dynamics, one only needs to consider an additional output, which can be written as

$$y_z(k) = \mathbf{C}_z\mathbf{x}(k),$$

with

$$\mathbf{C}_z = \begin{bmatrix} 0 & 0 & 1 & \mathbf{0}_{1\times 3} & 0 & 0 & \mathbf{0}_{1\times C_2^L} \end{bmatrix} \in \mathbb{R}^{1\times\left(3+3+1+1+C_2^L\right)}.$$

The rank condition is similar to (16) but with $\mathbf{L}_1$ replaced by

$$\mathbf{L}_1^z := 2\begin{bmatrix} s_{x,1} - s_{x,2} & s_{y,1} - s_{y,2} \\ s_{x,1} - s_{x,3} & s_{y,1} - s_{y,3} \\ \vdots & \\ s_{x,L-2} - s_{x,L} & s_{y,L-2} - s_{y,L} \\ s_{x,L-1} - s_{x,L} & s_{y,L-1} - s_{y,L} \end{bmatrix} \in \mathbb{R}^{C_2^L\times 2},$$

with $\mathbf{s}_i = \begin{bmatrix} s_{x,i} & s_{y,i} & s_{z,i} \end{bmatrix}^T$, $i = 1, \ldots, L$. The proofs of observability are similar but considering the additional output, which allows to show that the z-coordinate of both the inertial position and the inertial current velocity is observable and identical in both systems, the original and the augmented.

3.3. Estimation solution with augmented states

3.3.1. Kalman filter

An observer (or filter) for the augmented system (15) readily gives estimates of $v_s^2(t_k)\,\mathbf{p}(t_k)$, $v_s^2(t_k)\,\mathbf{v}_c(t_k)$, $v_s^2(t_k)$, and $b_c(t_k)$. As it was seen, the system dynamics (15) can be regarded as linear for observer (of filter) design purposes. A Kalman filter is an obvious choice, yielding globally exponentially stable error dynamics if the system is shown to be uniformly completely observable [35]. This will be detailed in the next theorem. An alternative to the Kalman filter could be the design of a Luenberger observer as detailed in [36, Theorem 29.2], which would allow one to choose the convergence rate. Before stating the uniform complete observability result, the following assumption is introduced.

Assumption 5. *The pseudo-range measurements $r_i(k)$, $i = 1, \ldots, L$, are bounded from below and from above. Moreover, the input $\mathbf{u}(k)$ is bounded from above.*

Again, the first is a technical assumption that can be easily verified in practice, similarly to Assumption 1. The second is also always true since the vehicles cannot achieve arbitrarily large linear velocities. Hence, these are mild assumptions. Notice that the specific bounds are not required and are arbitrary, as long as they exist.

Theorem 3. *Let k_0 denote the initial discrete-time instant and suppose that there exists a positive constant $B_L > 0$ such that*

$$\sigma_{min}\left(\mathbf{L}\left(k\right)\right) \geq B_L \tag{29}$$

for all $k \geq k_0$, where $\sigma_{min}(\mathbf{X})$ is the smallest singular value of $\mathbf{X}$. Then, the pair $(\mathbf{A}(k), \mathbf{C}(k))$ is uniformly completely observable.

Proof. The pair $(\mathbf{A}(k), \mathbf{C}(k))$ is uniformly completely observable if and only if there exist positive constants α, $\beta > 0$ and $N \in \mathbb{Z}$ such that, for all $k \geq k_0$,

$$\alpha\mathbf{I} \preceq \boldsymbol{\mathcal{I}}\left(k, k+N\right) \preceq \beta\mathbf{I}, \tag{30}$$

with

$$\boldsymbol{\mathcal{I}}\left(k, k+N\right) = \sum_{i=k}^{k+N} \boldsymbol{\phi}^T\left(i, k+N\right)\mathbf{C}^T(i)\mathbf{C}(i)\boldsymbol{\phi}\left(i, k+N\right),$$

where $\boldsymbol{\phi}(k, k_0)$ is the transition matrix associated with $\mathbf{A}(k)$ from k_0 to k. Fix $N = 1$. In this case,

$$\begin{aligned}\boldsymbol{\mathcal{I}}\left(k, k+1\right) &= \boldsymbol{\phi}^T\left(k, k+1\right)\mathbf{C}^T(k)\mathbf{C}(k)\boldsymbol{\phi}\left(k, k+1\right) \\ &\quad + \mathbf{C}^T(k+1)\mathbf{C}(k+1).\end{aligned}$$

As $\boldsymbol{\phi}(k+1, k) = \mathbf{A}(k)$, then it is possible to rewrite (30) as

$$\alpha\mathbf{I} \preceq \mathbf{A}^{-T}(k)\mathbf{C}^T(k)\mathbf{C}(k)\mathbf{A}^{-1}(k) + \mathbf{C}^T(k+1)\mathbf{C}(k+1) \preceq \beta\mathbf{I}. \tag{31}$$

Given the structure of $\mathbf{A}(k)$, its inverse is simply given by

$$\mathbf{A}^{-1} = \left[\begin{array}{cccc|c} \mathbf{I}_3 & -T\mathbf{I}_3 & -\mathbf{u} & \mathbf{0}_{3\times 1} & \mathbf{0}_{3\times C_2^L} \\ \mathbf{0}_3 & \mathbf{I}_3 & \mathbf{0}_{3\times_1} & \mathbf{0}_{3\times_1} & \mathbf{0}_{3\times C_2^L} \\ \mathbf{0}_{1\times 3} & \mathbf{0}_{1\times 3} & 1 & 0 & \mathbf{0}_{1\times C_2^L} \\ \mathbf{0}_{1\times 3} & \mathbf{0}_{1\times 3} & 0 & 1 & \mathbf{0}_{1\times C_2^L} \\ \hline \mathbf{0}_{C_2^L\times 3} & -\mathbf{A}_{55}^{-1}\mathbf{A}_{52} & -\mathbf{A}_{55}^{-1}\mathbf{A}_{53} & -\mathbf{A}_{55}^{-1}\mathbf{A}_{54} & \mathbf{A}_{55}^{-1} \end{array}\right],$$

where the time dependence was omitted for the sake of ease of presentation. Under the current assumptions, all quantities are bounded and hence the right side of (31) is easily verified. To simplify the remainder of the proof, notice that, since $\mathbf{A}(k)$ is nonsingular, with singular values bounded from above and from below, to show the left side of (31) is equivalent to show that there exists a positive constant $\alpha' > 0$ such that

$$\alpha'\mathbf{I} \preceq \mathbf{C}^T(k)\mathbf{C}(k) + \mathbf{A}^T(k)\mathbf{C}^T(k+1)\mathbf{C}(k+1)\mathbf{A}(k)$$

for all $k \geq k_0$. Moreover, this is equivalent, attending to the definition of positive semi-definite matrix, to show that there exists $\alpha' > 0$ such that, for all $k \geq k_0$ and all unit vectors $\mathbf{d} = \left[\begin{array}{ccccc} \mathbf{d}_1^T & \mathbf{d}_2^T & d_3 & d_4 & \mathbf{d}_5^T \end{array}\right]^T \in \mathbb{R}^{3+3+1+1+C_2^L}$, with $\mathbf{d}_1, \mathbf{d}_2 \in \mathbb{R}^3$, $d_3, d_4 \in \mathbb{R}$, $\mathbf{d}_5 \in \mathbb{R}^{C_2^L}$, it is true that

$$w(k) \geq \alpha', \tag{32}$$

where $w(k) := \|\mathbf{C}(k)\mathbf{d}\|^2 + \|\mathbf{C}(k+1)\mathbf{A}(k)\mathbf{d}\|^2$. It is a simple matter of computation to show that

$$\mathbf{C}(k)\mathbf{d} = \left[\begin{array}{c} \mathbf{d}_5 \\ \mathbf{o}_1(k) \end{array}\right]$$

and

$$\mathbf{C}(k+1)\mathbf{A}(k)\mathbf{d} = \left[\begin{array}{c} \mathbf{o}_2(k) \\ \mathbf{o}_3(k) \end{array}\right],$$

where

$$\mathbf{o}_1(k) = \mathbf{E}^{-1}(k)\mathbf{L}(k)\left[\begin{array}{c} \mathbf{d}_1 \\ d_3 \\ d_4 \end{array}\right] + \mathbf{d}_5,$$

$$\mathbf{o}_3(k) = -T\mathbf{E}^{-1}(k+1)\mathbf{L}_1\mathbf{d}_2 + \mathbf{A}_{53}(k)\mathbf{d}_3 + \mathbf{A}_{54}(k)\mathbf{d}_4 + \mathbf{A}_{55}(k)\mathbf{d}_5,$$

and $\mathbf{o}_2(k)$ is omitted since it is not needed. Notice that, under the assumptions of the paper, all quantities in $\mathbf{o}_3(k)$ are bounded. Moreover, recall that $\mathbf{d}$ is a unit vector, hence the larger $\|\mathbf{d}_2\|$ is, the smaller $|d_3|$, $|d_4|$, and $\|\mathbf{d}_5\|$ must be. Using also (29), it is possible to conclude that there exists $0 < \epsilon_1 < 1$ such that, for all $\|\mathbf{d}_2\| \geq \epsilon_1$, it follows that $\|\mathbf{o}_3(k)\| \geq \alpha_1 > 0$. The remainder of the proof follows by exhaustion, considering all the possible unit vectors $\mathbf{d}$. Fix an arbitrary $k \geq k_0$ and consider the case $\epsilon_1 \leq \|\mathbf{d}_2\| \leq 1$. Thus, $\|\mathbf{o}_3(k)\| \geq \alpha_1$ and using simple norm inequalities, it is readily concluded that $\|\mathbf{C}(k+1)\mathbf{A}(k)\mathbf{d}\| \geq \alpha_1$, and hence $w(k) \geq \alpha_1^2$. Suppose now that $\|\mathbf{d}_2\| < \epsilon_1$. Since $\mathbf{d}$ is a unit vector, it must be

$$\sqrt{1-\epsilon_1^2} < \left\|\left[\begin{array}{cccc} \mathbf{d}_1^T & d_3 & d_4 & \mathbf{d}_5^T \end{array}\right]^T\right\| \leq 1.$$

Now, notice that all quantities in $\mathbf{o}_1(k)$ are bounded. Moreover, recall that $\mathbf{d}$ is a unit vector and it is now assumed that $\|\mathbf{d}_2\| < \epsilon_1$. Hence the smaller $\|\mathbf{d}_5\|$ is, the larger $\left\|\left[\begin{array}{ccc} \mathbf{d}_1^T & d_3 & d_4 \end{array}\right]^T\right\|$ must be. Using also (29), it is possible to conclude that there exists $0 < \epsilon_2 < 1$ such that, for all $\|\mathbf{d}_2\| < \epsilon_1$ and $\|\mathbf{d}_5\| < \epsilon_2$, it follows that $\|\mathbf{o}_1(k)\| \geq \alpha_2 > 0$. As a result, $\|\mathbf{C}(k)\mathbf{d}\| \geq \alpha_2$ and $w(k) \geq \alpha_2^2$. Finally, suppose that $\|\mathbf{d}_2\| < \epsilon_1$ and $\|\mathbf{d}_5\| \geq \epsilon_2$. In this case, it is trivial to see that $\|\mathbf{C}(k)\mathbf{d}\| \geq \epsilon_2$ and hence $w(k) \geq \epsilon_2^2$. This concludes the proof since (32) holds for all unit vectors $\mathbf{d}$, with $\alpha' := \min\left(\alpha_1^2, \alpha_2^2, \epsilon_2^2\right)$. □

3.3.2. Slowly time-varying quantities

In nominal terms, and for modeling purposes, the ocean current velocity, the factor that accounts for the unknown sound speed velocity, and the clock offset are assumed constant. Nevertheless, it is possible, by appropriate tuning of the Kalman filter, to successfully track slowly time-varying quantities, as it will be shown in the simulations. In the case of the ocean currents, it is important to stress that it is the ocean current that the vehicle experiences that matters. Thus, from the vehicle's perspective, the ocean current might change even if at each fixed

inertial position the ocean current profile is constant. This is because the vehicle may translate through ocean currents which change spatially. For the particular treatment of ocean currents see e.g. [37] and [38].

3.3.3. Estimation between range measurements

An observer (or filter) for the discrete-time system (15) only provides estimates when pseudo-range measurements are available. However, the DVL and the AHRS usually provide data at higher rates. Hence, estimation at a higher rate can be achieved by dead reckoning between pseudo-range measurements, as given by

$$\begin{cases} \hat{\mathbf{x}}_1(t) = \hat{\mathbf{x}}_1(t_k) + (t-t_k)\,\hat{\mathbf{x}}_2(t_k) + \hat{x}_3(t_k)\int_{t_k}^{t} \mathbf{R}(\tau)\,\mathbf{v}_r(\tau)\,d\tau \\ \hat{\mathbf{x}}_2(t) = \hat{\mathbf{x}}_2(t_k) \\ \hat{x}_3(t) = \hat{x}_3(t_k) \\ \hat{x}_4(t) = \hat{x}_4(t_k) \end{cases} \tag{33}$$

for $t_k < t < t_{k+1}$.

3.3.4. Estimates of $\mathbf{p}(t)$, $\mathbf{v}_c(t)$, and $v_s(t)$

The estimates provided by an observer (or filter) for the augmented system (15) do not correspond exactly to the desired ones, as the inertial position and ocean current velocity are scaled and the factor $v_s(t)$ is squared. Nevertheless, estimates for $\mathbf{p}(t_k)$, $\mathbf{v}_c(t_k)$, and $v_s(t)$ follow from the Kalman filter or the Luenberger observer estimates, under some mild assumptions. As this has been detailed in [32], only the main results are shown.

Assumption 6. *Upper and lower bounds on the speed of propagation of the acoustic waves in the medium exist such that the scaling factor $v_s(t)$ satisfies*

$$V_m \leq v_s(t) \leq V_M,$$

with $V_m, V_M > 0$.

Assumption 7. *The inertial position of the vehicle and the ocean current velocity are norm-bounded.*

Considering estimates $\hat{x}_3(t)$ with globally exponentially stable error dynamics, the estimate of the ratio between the nominal speed assumed by the range sensor and the actual speed of propagation of the acoustic waves in the medium can be obtained from

$$\hat{v}_s(t) = \begin{cases} V_m, & \hat{x}_3(t) < V_m^2 \\ \sqrt{\hat{x}_3(t)}, & V_m^2 \leq \hat{x}_3(t) \leq V_M^2 \\ V_M, & \hat{x}_3(t) > V_M^2 \end{cases}, \tag{34}$$

whose error also converges exponentially fast to zero for all initial conditions under Assumption 6. Estimates for the position and ocean current velocity then follow from

$$\begin{cases} \hat{\mathbf{p}}(t) = \frac{\hat{\mathbf{x}}_1(t)}{\hat{v}_s^2(t)} \\ \hat{\mathbf{v}}_c(t) = \frac{\hat{\mathbf{x}}_2(t)}{\hat{v}_s^2(t)} \end{cases}, \tag{35}$$

and it is possible to show that, under Assumptions 6 and 7, these also converge exponentially fast to zero for all initial conditions, see [32, Proposition 1].

3.4. Estimation solution without state augmentation

As it will be seen, it is interesting to include the augmented states in the system for filtering purposes. However, it should be recognized that a simpler solution exists without state augmentation. Indeed, define the reduced system state

$$\mathbf{x}_r(k) := \begin{bmatrix} \mathbf{x}_1(k) \\ \mathbf{x}_2(k) \\ x_3(k) \\ x_4(k) \end{bmatrix} \in \mathbb{R}^8.$$

Based on (7) and (12), it is possible to write

$$\begin{cases} \mathbf{x}_r(k+1) = \mathbf{A}_r(k)\mathbf{x}(k) \\ \mathbf{y}_r(k) = \mathbf{C}_r(k) \end{cases}, \tag{36}$$

where $\mathbf{A}_r(k) \in \mathbb{R}^{8\times 8}$ is evident from the context, corresponding to the upper left block of $\mathbf{A}(k)$, $\mathbf{y}_r(k) \in \mathbb{R}^{C_2^L}$ corresponds to the pseudo-range differences, and

$$\mathbf{C}_r(k) = -\begin{bmatrix} \mathbf{C}_{21}(k) & \mathbf{0}_{C_2^L\times 3} & \mathbf{C}_{23}(k) & \mathbf{C}_{24}(k) \end{bmatrix}$$

encodes the LBL structure (12). It is easily concluded that all the observability results apply to (36) since the missing states are directly measured in (15).

4. Simulation results

In order to evaluate the performance of the novel OWTT LBL solution, simulation results resorting to the Monte Carlo method are presented herein. In Section 4.1 the simulation setup is introduced, whereas a theoretical performance limit is described in Section 4.2. The proposed solutions are detailed in Section 4.3, whereas the EKF is briefly described in Section 4.4. Finally, extensive Monte Carlo runs are detailed and discussed in Section 4.5, where the comparison with the theoretical performance bound is also performed.

4.1. Setup

In the simulations the vehicle describes the trajectory depicted in Fig. 1. Its initial position is $\mathbf{p}(0) = [0\,0\,10]^T$ m, whereas the inertial ocean current velocity was set to $\mathbf{v}_c(0) = [0.1\ -0.2\,0]^T$ m/s. Five acoustic fixed pingers are considered, whose inertial positions are $\mathbf{s}_1 = \begin{bmatrix} 0 & 0 & 0 \end{bmatrix}^T$ m, $\mathbf{s}_2 = \begin{bmatrix} 1000 & 0 & 500 \end{bmatrix}$m, $\mathbf{s}_3 = \begin{bmatrix} 0 & 750 & 500 \end{bmatrix}$m, $\mathbf{s}_4, = \begin{bmatrix} 500 & 0 & 500 \end{bmatrix}$m, and $\mathbf{s}_5 = \begin{bmatrix} 0 & 0 & 500 \end{bmatrix}$m. Notice that, with this configuration, the observability condition (16) is verified; hence both Theorems 1 and 2 apply. The scale factor that accounts for the unknown speed of propagation of the sound was set to $v_s = 1.05$. As an example, this means that if the actual speed of propagation was 1500 m/s, the nominal speed considered by the acoustic positioning system would be 1575 m/s. The term that accounts for the offset between clocks was set to $b_c = 50$ m. As an example, this corresponds to a clock offset of $50/1500 \approx 33.3\times 10^{-3}$ s for a nominal speed of propagation assumed by the acoustic positioning system of 1500 m/s.

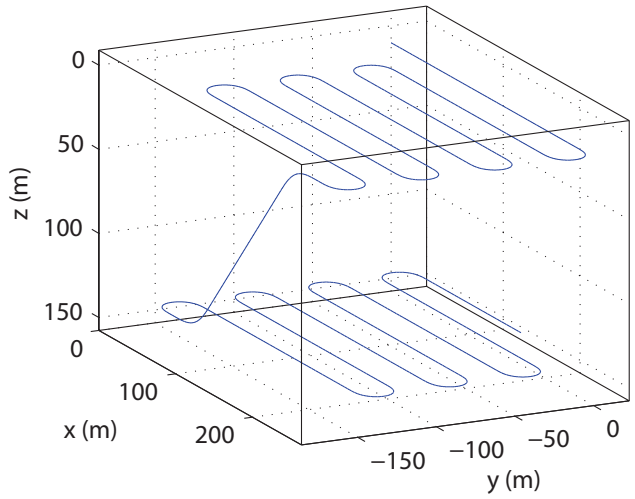

Figure 1: Trajectory described by the vehicle

Sensor noise was considered in the simulations for all sensors. In particular, the pseudo-distance readings are perturbed by zero-mean additive Gaussian noise, with standard deviation of 1 m, whereas the relative velocity measurements provided by the DVL are assumed perturbed by additive zero-mean Gaussian noise, with standard deviation of 0.01 m/s. The attitude of the vehicle is assumed parametrized by roll, pitch, and yaw Euler angles, also corrupted by additive zero-mean Gaussian noise, with standard deviation of 0.03° for the roll and pitch and 0.3° for the yaw.

In underwater applications, acoustic transmission cannot be carried out at high rates. In the simulations, the sampling period for the pseudo-ranges was set to $T = 10\,\mathrm{s}$, simulating hard conditions, whereas the remaining sensors are sampled with a frequency of 5 Hz, which corresponds to a sampling period of $T_f = 0.2$ s. The discrete-time input $\mathbf{u}(k)$, which corresponds to a definite integral, was approximated using the trapezoid rule, while the open-loop solution of the position estimates, between pseudo-range measurements, was approximated using the Euler method.

4.2. Bayesian Cramér-Rao bound

Although the design of optimal estimators for nonlinear systems is still an open area of research (and will probably remain so as some of the problems might be intractable), it is possible to compute, in some cases, theoretical bounds for the achievable performance. In particular, for discrete-time systems with linear process dynamics and nonlinear outputs, and considering zero-mean additive Gaussian noise, it is possible to compute the Bayesian Cramér-Rao Bound (BCRB), which gives a lower limit for the covariance matrix of the estimation error of any causal (realizable) unbiased estimator [39].

Consider the discrete-time nonlinear system

$$\begin{cases} \mathbf{x}(k+1) = \mathbf{F}(k)\mathbf{x}(k) + \mathbf{B}(k)\mathbf{u}(k) + \mathbf{n}_x(k) \\ \mathbf{y}(k) = \mathbf{h}\left(\mathbf{x}(k)\right) + \mathbf{n}_y(k) \end{cases}, \tag{37}$$

where $\mathbf{x}(k)$ denotes the state of the system, $\mathbf{u}(k)$ is a deterministic input, $\mathbf{y}(k)$ is the output of the system, $\mathbf{h}\left(\mathbf{x}(k)\right)$ is a nonlinear function of the system state, $\mathbf{n}_x(k)$ is a zero-mean Gaussian process with covariance $\mathbf{Q}_x(k)$, and $\mathbf{n}_y(k)$ is also a zero-mean Gaussian process with covariance $\mathbf{Q}_y(k)$. The recursion that describes the BCRB is similar to that of the covariance of the EKF, with the difference that the Jacobian of $\mathbf{h}\left(\mathbf{x}(k+1)\right)$ is evaluated at the true state of the system, see [39, Section 2.3.3]. Using the information matrix representation, the BCRB is given by $\mathbf{P}_L(k) = \mathbf{J}^{-1}(k)$, where $\mathbf{J}(k)$ satisfies the recursion

$$\mathbf{J}(k+1) = \left[\mathbf{Q}_x\left(k\right) + \mathbf{F}\left(k\right)\mathbf{J}^{-1}\left(k\right)\mathbf{F}^T\left(k\right)\right]^{-1} + \mathbf{P}_m\left(k+1\right).$$

Here, the term $\mathbf{P}_m\left(k+1\right)$ is related to the reduction of the covariance due to the observations and is given by

$$\mathbf{P}_m(k+1) = E_{\mathbf{x}(k+1)}\left\{\tilde{\mathbf{H}}^T\left(\mathbf{x}\left(k+1\right)\right)\mathbf{Q}_y^{-1}(k+1)\,\tilde{\mathbf{H}}\left(\mathbf{x}\left(k+1\right)\right)\right\}, \tag{38}$$

where $\tilde{\mathbf{H}}\left(\mathbf{x}\left(k+1\right)\right)$ is the Jacobian of the nonlinear output function evaluated at $\mathbf{x}(k+1)$.

The expected value in (38) is computed with respect to the state vector $\mathbf{x}(k+1)$ and therefore it is usually approximated resorting to the Monte Carlo method. In nonlinear estimation problems, as the one addressed in this paper, it is often interesting to evaluate the performance along nominal state trajectories $\overline{\mathbf{x}}(k)$. In this case, the term $\mathbf{P}_m(k+1)$ may be simplified, as given by

$$\mathbf{P}_m(k+1) = \tilde{\mathbf{H}}^T\left(\overline{\mathbf{x}}(k+1)\right)\mathbf{Q}_y^{-1}(k+1)\,\tilde{\mathbf{H}}\left(\overline{\mathbf{x}}(k+1)\right),$$

which allows for the evaluation of the performance of an estimator given the specific structure of the problem. The resulting equations are identical to those of the information version of the extended Kalman filter and the Jacobians are computed along nominal state trajectories $\overline{\mathbf{x}}(k)$ instead of the estimated trajectories, as detailed in [39].

The nonlinear system (5) has the same form of (37). Therefore, it is possible to compute, in this case, a theoretical bound on the best possible achievable performance by an unbiased causal estimator. It is important to stress, however, that this only gives a bound, not necessarily achievable by the best unbiased estimator.

4.3. Proposed solution

As described in Section 3.3, the solution proposed in this paper for the problem of navigation based on pseudo-range measurements consists in applying a discrete-time Kalman filter to (15), with open-loop propagation between pseudo-range measurements given by (33). The final estimates for the inertial position and ocean current velocity are given by (35), whereas the estimate of the factor that accounts for the unknown speed of propagation is computed using (34).

The covariance matrix related to the perturbations in the state equation was chosen as

$$\mathbf{diag}\left(0.01^2\frac{\mathrm{T}}{\mathrm{T_f}}\mathbf{I}_3,\, 0.001^2\mathbf{I}_3,\, 0.01^2,\, 0.01^2,\, 10^{-4}\mathbf{I}_{\mathrm{C}_2^{\mathrm{L}}}\right).$$

Here, the first factor accounts for the standard deviation of the open-loop integration of noisy relative velocity readings rotated by noisy attitude measurements, which are obtained with

a sampling period of T_f, between pseudo-range measurements, which are obtained with a period of T, whereas 0.01 corresponds to the standard deviation of the noise of the relative velocity measurements. The second block corresponds to a small value as the ocean current velocity is assumed constant. This value is not zero to ensure that the system is controllable from the noise affecting that particular state equation. Otherwise, the convergence speed of the Kalman filter would be very small. The same goes for the third and fourth blocks, which correspond to the state disturbance noise affecting the factor that account for the unknown speed of propagation of the acoustic waves and the clock offset, both assumed constant. The last parameter was chosen empirically, which is nevertheless common for nonlinear estimation problems as it is this case.

In addition to the solution proposed in Section 3.3, is is possible to implement an alternative filter with fewer states, not including the pseudo-range differences in the system state, as briefly described in Section 3.4. In this case, the covariance matrix related to the perturbations in the state equation was chosen as before discarding the component related to the pseudo-range differences, as given by

$$\mathbf{diag}\left(0.01^2\frac{\mathrm{T}}{\mathrm{T_f}}\mathbf{I}_3,\, 0.001^2\mathbf{I}_3,\, 0.01^2,\, 0.01^2\right).$$

Ignoring the cross correlation between pseudo-range differences, the output noise covariance was chosen as $\mathbf{diag}\left(2\mathbf{I}_{\mathrm{C_2^L}},\, 0.2\mathbf{I}_{\mathrm{C_2^L}}\right)$ for the solution with augmented states, proposed in Section 3.3. The first block corresponds to twice the variance of the pseudo-range measurements (the output corresponds to the differences), whereas the second block was chosen empirically. For the solution without the pseudo-range differences included in the system state, detailed in Section 3.4, the output noise covariance was chosen as $2\mathbf{I}_{C_2^L}$. Notice that cross-correlation terms can also be considered, leading to alternative tuning parameters. In that case, when two outputs are correlated, e.g. $r_1(k) - r_2(k)$ and $r_1(k) - r_3(k)$, the cross correlation term of the output noise covariance matrix was set to 0.9. Finally, notice that when all combinations of pseudo-ranges are included, as detailed in Section 3, there is some redundancy. As an example,

$$r_2(k) - r3(k) = -\left[r_1(k) - r_2(k)\right] + \left[r_1(k) - r_3(k)\right].$$

Hence, a reduced set of combinations can be considered, e.g. using only the differences to the first pseudo-range measurement. All in all, these choices lead to eight different alternative designs, as detailed in Table 1. To summarize: i) two different system states can be considered, with state augmentation including the pseudo-range differences in the system state (Section 3.3), or without state augmentation (Section 3.4): ii) it is possible to consider all combinations of differences of pseudo-ranges, or just the differences to the first pseudo-range; and iii) it is possible to consider cross correlation terms, or ignore these.

4.4. Extended Kalman filter

The EKF is one of the most commonly used estimation solutions for nonlinear systems [40], albeit no guarantees of global asymptotic stability are offered. In fact, that is one of the reasons that has led the community to pursue alternative approaches. Nevertheless, it often offers very good performance. For this reason, simulation results are also presented using an EKF applied to the nonlinear system (5).

Table 1: Filters description

Filter id	Augmented states	Pseudo-range combinations	Cross correlation
#1	Yes	All	No
#2	Yes	All	Yes
#3	Yes	Minimum	No
#4	Yes	Minimum	Yes
#5	No	All	No
#6	No	All	Yes
#7	No	Minimum	No
#8	No	Minimum	Yes

For the EKF, the covariance matrices were chosen as before but discarding the terms related to the additional states and outputs, as the EKF is directly applied to the original nonlinear system (5). Hence, the state disturbance covariance matrix was set to $\mathbf{diag}\left(0.01^2\frac{\mathrm{T}}{\mathrm{T_f}}\mathbf{I}_3,\, 0.001^2\mathbf{I}_3,\, 0.01^2,\, 0.01^2\right)$. The output noise covariance matrix is given by $\mathbf{I}_L$, in accordance with the standard deviation of the noise of the pseudo-range measurements.

4.5. Monte Carlo runs

In order to characterize the performance of the proposed solution, the Monte Carlo method was applied. In particular, 1000 runs were carried out for the scenario described in Section 4.1 for all filters described in Section 4.3. In addition to the results considering the eight setups defined in Table 1, the EKF results are also included, as well as the BCRB described in Section 4.2. Hence, it is possible to compare the proposed solution with both the EKF and a theoretical performance limit.

The initial estimate for the filters, in each run, follows a Gaussian distribution centered at the true value and with standard deviation of 200 m for the position, 1 m/s for the ocean current velocity, 0.1 for the factor that accounts for the unknown speed of propagation of the acoustic waves in the medium, and 50 m for the bias resulting from the clock offset. The states corresponding to the pseudo-range differences were initialized according to the first set of measurements, as these are available. The distributions of initial states that are considered are centered at the true value because the goal here is to evaluate the performance, not the convergence. The latter was already established for the proposed solution, whereas the EKF offers no guarantees. In fact, there were simulations in which the EKF did not converge, as it will be shortly detailed. These were simply discarded when presenting the Monte Carlo results.

The initial Kalman filter covariance was chosen as $\mathbf{diag}\left(200^2\mathbf{I}_3,\, \mathbf{I}_3,\, 0.1^2,\, 50^2, \mathbf{I}_{\mathrm{C_2^L}}\right)$ for the proposed solution. For the Kalman filter without state augmentation and the EKF, it was set to $\mathbf{diag}\left(200^2\mathbf{I}_3,\, \mathbf{I}_3,\, 0.1^2,\, 50^2\right)$. These are in accordance

with the initial distribution of the error that is considered in the 1000 Monte Carlo runs.

For each time instant, the root-mean-square-errors (RMSE) were computed for all quantities and all the solutions that were tested, including the EKF. These are also compared with the standard deviation that results from the BCRB, which corresponds to the square root of the diagonal elements of $\mathbf{P}_L(k)$. To compute the BCRB, the state disturbance covariace was set to $\mathbf{diag}\left(0.01^2\frac{\mathrm{T}}{\mathrm{T_f}}\mathbf{I}_3, \mathbf{0}_3, 0, 0\right)$. In Fig. 2 the RMSE results for the x-component of the position are shown, whereas the RMSE results for the x-component of the ocean current velocity error are depicted in Fig. 3. The results for the y and z components are similar and hence omitted. In these figures, the theoretical performance bound is shown in black (BCRB). The RMSE results for the factors that account of the speed of propagation and the clock offset are depicted in Figs. 4 and 5, respectively.

In terms of initial evolution, two conclusions can be drawn: i) the EKF offers the worst performance; and ii) the solution with the augmented state offers the best performance. Nevertheless, after five minutes, the RMSE are all within very reasonable values for all solutions but the EKF, close to steady-state.

With respect to the steady-state evolution, it is interesting to see that, again, the EKF offers the worst performance, followed by the solution without state augmentation detailed in Section 3.4. Indeed, the solution with state augmentation, derived in detail in the paper, offers the best performance. Considering the cross-correlation between output measurements does not seem to have a significant positive influence. In fact, the filter that offers here the best performance is #3. In this first set of Monte Carlo runs, it does not seem to be advantageous to consider all the possible combinations of pseudo-range differences. However, it will be shown shortly that this can also be beneficial.

In addition to these plots, the average of the RMSE was computed for each variable from 1800 s to 3600 s. The results are shown in Table 2. Again, the results for the y and z coordinates of the position and inertial current velocity are similar to the x component and therefore omitted.

Table 2: Average steady-state RMSE

Filter	p_x (m)	v_x (m/s)	v_s	b_c (m)
#1	0.365	0.0026	1.05×10^{-3}	1.674
#2	0.347	0.0023	1.00×10^{-3}	1.599
#3	0.310	0.0019	0.78×10^{-3}	1.172
#4	0.344	0.0021	1.00×10^{-3}	1.594
#5	0.552	0.0028	1.53×10^{-3}	1.890
#6	0.552	0.0027	1.49×10^{-3}	1.850
#7	0.482	0.0019	1.34×10^{-3}	1.636
#8	0.527	0.0024	1.46×10^{-3}	1.770
EKF	0.802	0.0029	1.92×10^{-3}	1.466
BCRB	0.248	0.0005	0.17×10^{-3}	0.089

As briefly mentioned, the EKF did not always converge. In particular, out of 1000 runs, the EKF failed in 6 of these. While this may seem a small number, for fully autonomous vehicles this is quite unacceptable as the failure of the navigation system could quickly endanger any mission. The proposed solution never failed, as theoretically expected. For the sake of completeness, an example of failure of the EKF is here shown. The initial condition is $\hat{\mathbf{p}}(0) \approx \begin{bmatrix} -334.4508 & 28.7651 & -511.4626 \end{bmatrix}$ (m), $\hat{\mathbf{v}}_c(0) \approx \begin{bmatrix} -1.6530 & -0.3151 & -0.3917 \end{bmatrix}$ (m/s), $\hat{v}_s(0) \approx 0.8071$, and $\hat{b}_c(0) \approx 44.7801$ m. The initial evolution of the EKF errors is depicted in Fig. 6. For comparison, the initial convergence of the estimation errors with the proposed solutions is shown in Fig. 7. Interestingly enough, it is also quite evident here the advantage of augmenting the state with the pseudo-range differences.

Besides the initial convergence and performance, it is also interesting to compare the computational cost of each solution. To that purpose, the computation time that 100 runs of each filter take is shown in Table 3. The laptop that was used has an Intel©Core i7 - 6500U processor with 16GB of RAM. While the EKF is the least expensive in terms of computation time and the proposed solution with state-augmentation and considering all the pseudo-range differences is the most expensive, the difference is small considering the benefits with respect to EKF, both in terms of convergence guarantees and performance. Indeed, the most expensive takes roughly 23% more time than the EKF. The proposed solution with state augmentation takes roughly 15% more time than the one without state augmentation, which is again a small price for the increased performance, both in terms of convergence time and steady-state performance. Finally, the solutions that consider all the combinations of pseudo-range differences take roughly 10% more time than the ones that consider only the differences to the first pseudo-range.

Table 3: Computation time for 100 simulations

Filter	Time (s)
#1	148.6
#2	148.1
#3	134.9
#4	134.3
#5	127.2
#6	126.6
#7	125.0
#8	125.2
EKF	120.7

In this first set of Monte Carlo runs, the ocean current velocity was kept constant, which corresponds to the nominal deterministic model that was assumed in the derivations in Section 3. Next, Monte Carlo results are shown for a time-varying ocean current in order to illustrate the robustness of the solution. The evolution of the ocean current velocity is now shown in Fig. 8, which was obtained considering the model

$$\mathbf{v}_c\left((k+1)T_f\right) = \mathbf{v}_c\left(kT_f\right) + \mathbf{n}_v(k),$$

where $\mathbf{n}_v$ is a zero-mean Gaussian process with covariance $0.001^2\mathbf{I}_3$. To compute the BCRB, the covariance state matrix was set to $\mathbf{diag}\left(0.01^2\frac{\mathrm{T}}{\mathrm{T_f}}\mathbf{I}_3, 0.001^2\mathbf{I}_3, 0.01^2, 0.01^2\right)$. All the remaining simulation parameters are as before.

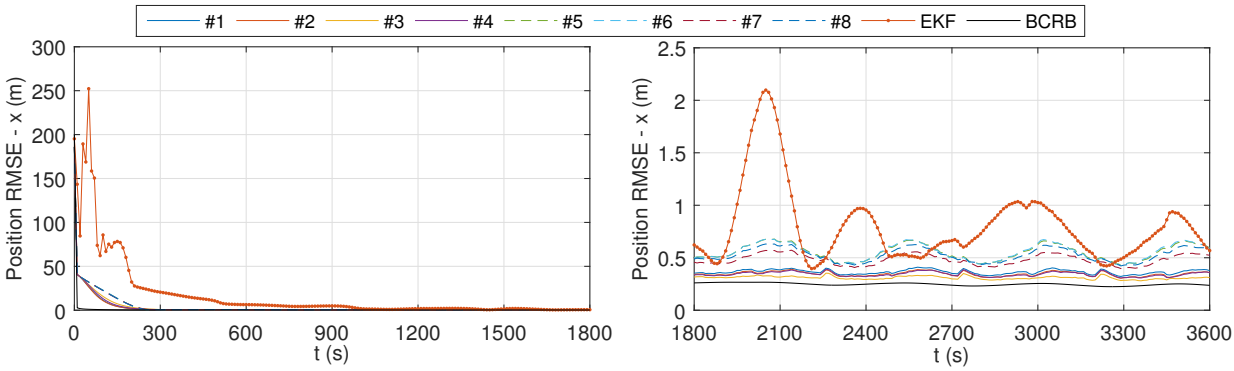

Figure 2: RMSE: x-coordinate of the position

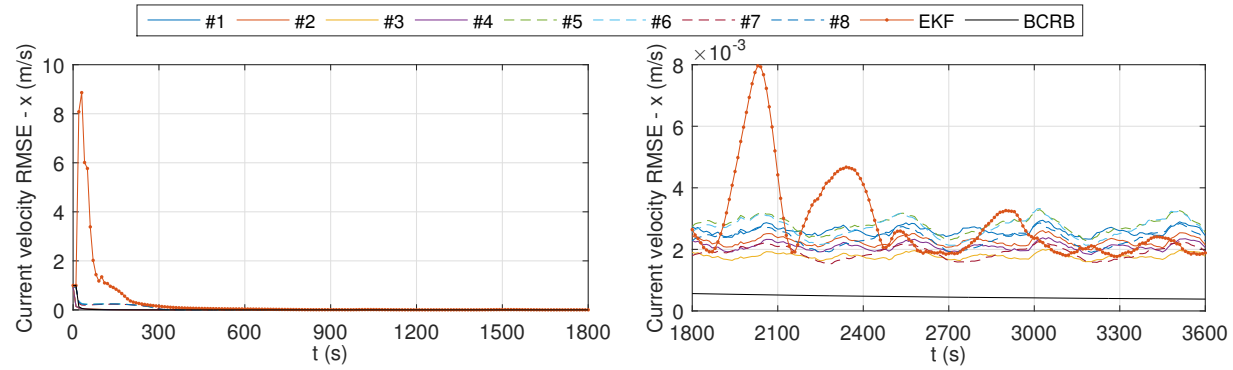

Figure 3: RMSE: x-coordinate of the inertial current velocity

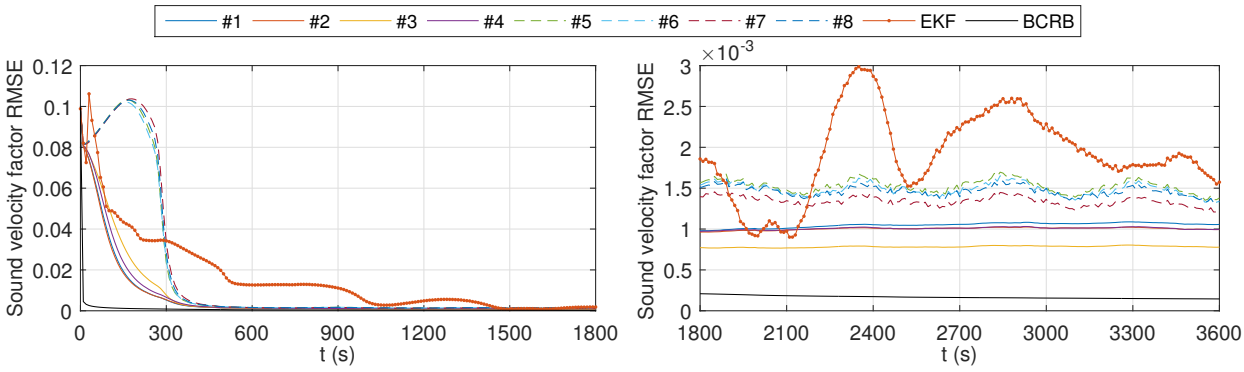

Figure 4: RMSE: sound velocity factor

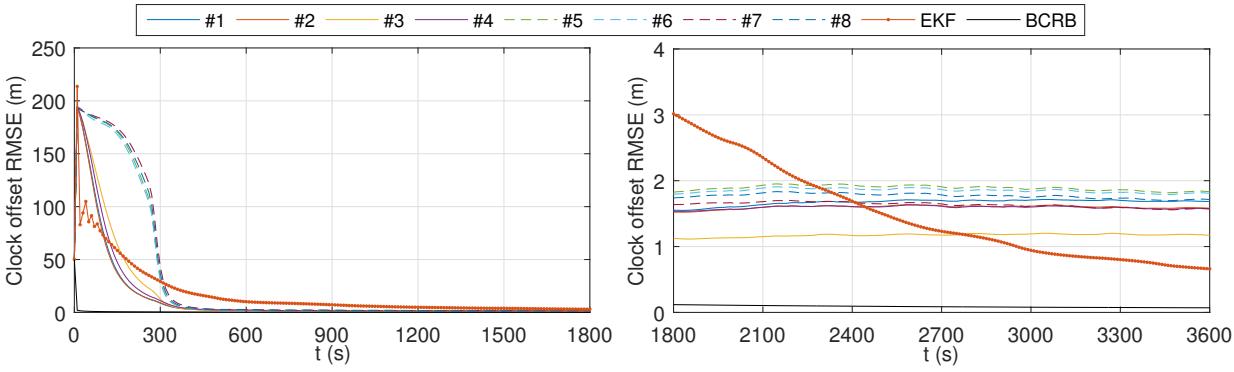

Figure 5: RMSE: clock offset factor

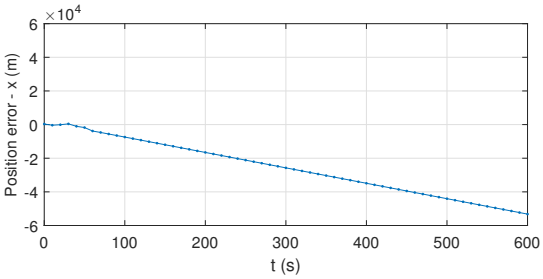

(a) Position: x-coordinate

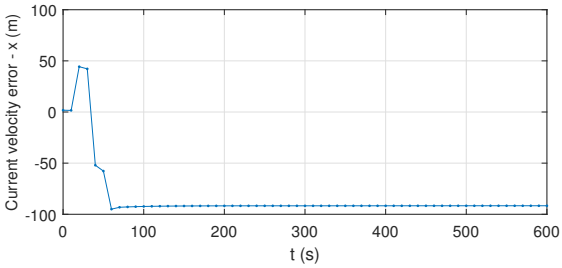

(b) Current velocity x-coordinate

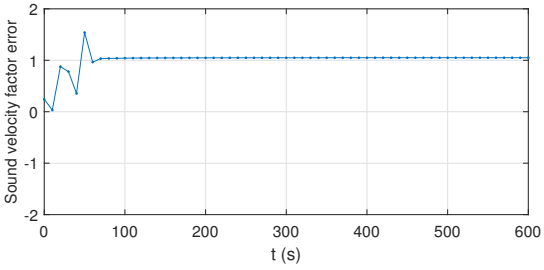

(c) Sound velocity factor

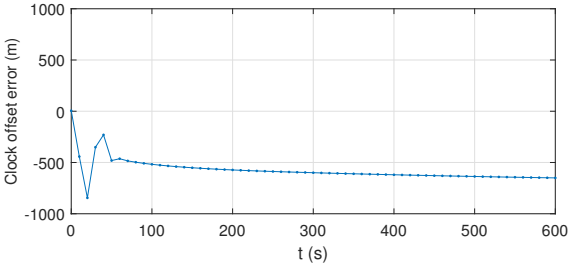

(d) Clock offset

Figure 6: EKF failure example: errors

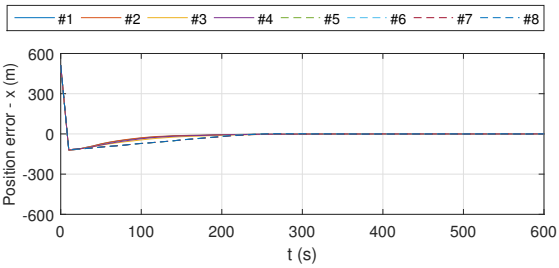

(a) Position: x-coordinate

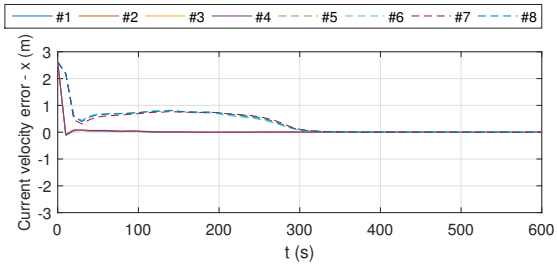

(b) Current velocity x-coordinate

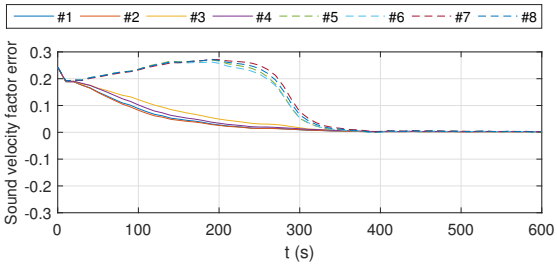

(c) Sound velocity factor

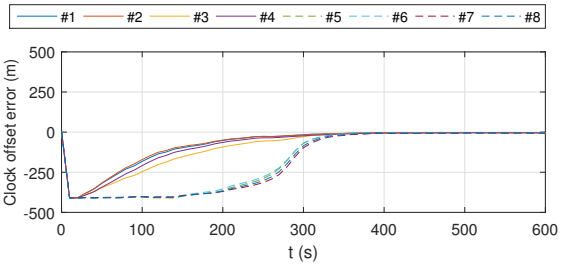

(d) Clock offset

Figure 7: Initial convergence of the proposed solution: errors

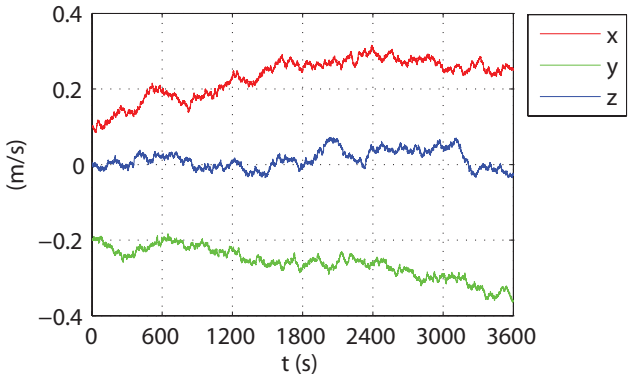

Figure 8: Evolution of the inertial ocean current velocity $\mathbf{v}_c(t)$

The initial evolution of the RMSE is very similar to the one presented before. Moreover, the form of the steady-state evolution of the RMSE is also similar but dwelling around higher values, as expected. Hence, plots are omitted. Again, the average of the RMSE was computed for each variable from 1800 s to 3600 s and the results are shown in Table 4. The results for the y and z coordinates of the position and inertial current velocity are similar to the x component and therefore these are omitted. The degradation in terms of estimation performance is evident and expected. The most distinct feature is that the solution with state augmentation and considering all the pseudo-range combinations now offers the best performance. Again, the filters without state augmentation offer lower performance than the ones with state augmentation. The EKF failed again in 6 simulations, with the same initial conditions.

Table 4: Average steady-state RMSE in the presence of time-varying ocean currents

Filter	p_x (m)	v_x (m/s)	v_s	b_c (m)
#1	0.989	0.0195	2.33×10^{-3}	3.883
#2	1.107	0.0205	2.26×10^{-3}	3.782
#3	1.380	0.0221	2.44×10^{-3}	4.060
#4	1.179	0.0210	2.40×10^{-3}	3.981
#5	1.587	0.0252	3.10×10^{-3}	3.652
#6	1.589	0.0254	3.17×10^{-3}	3.678
#7	2.251	0.0284	3.96×10^{-3}	3.993
#8	1.812	0.0265	3.39×10^{-3}	3.787
EKF	1.707	0.0236	2.29×10^{-3}	1.491
BCRB	0.474	0.0041	0.94×10^{-3}	0.125

5. Conclusions

A novel concept for long baseline navigation in a one-way-travel-time operational mode was proposed in this paper. It departs from previous approaches in that: i) the clock of the receiver mounted on-board the vehicle does not need to be synchronized with the clocks of the emitters; and ii) the speed of propagation of the signals is assumed unknown. This significantly lowers the operational burden and hardware requirements in LBL navigation. In the proposed framework, the system dynamics were written in a continuous-discrete time framework, so that pseudo-range measurements, obtained at low update rates, are used to drive the estimation error to zero, while others sensors, which operate at higher rates, are used to drive the system dynamics. An augmented linear system was then derived its observability and equivalence to the original system were established under appropriate conditions. A Kalman filter is proposed as the estimation solution, yielding globally exponentially stable error dynamics. Finally, extensive simulations were carried out resorting to Monte Carlo runs that demonstrate the performance of the proposed solution. A comparison with the EKF is also included, as well as with the BCRB.

Acknowledgments

The author would like to acknowledge the valuable discussions and suggestions of Profs. Carlos Silvestre and Paulo Oliveira mainly during the first phases of development of this work.

This work was supported by the Fundação para a Ciência e a Tecnologia (FCT) through ISR under FCT [UID/EEA/50009/2013].

References

[1] M. Hunt, W. Marquet, D. Moller, K. Peal, W. Smith, R. Spindel, An acoustic navigation system, Tech. Rep. Technical Report 74-6, Woods Hole Oceanographic Institution (Dec. 1974).

[2] P. Milne, Underwater Acoustic Positioning Systems, Gulf Publishing Co, 1983.

[3] L. Techy, K. Morgansen, C. Woolsey, Long-baseline acoustic localization of the Seaglider underwater glider, in: Proceedings of the 2011 American Control Conference, San Francisco, USA, 2011, pp. 3990–3995.

[4] L. Whitcomb, D. Yoerger, H. Singh, Combined Doppler/LBL Based Navigation of Underwater Vehicles, in: Proceedings of the 11th International Symposium on Unmanned Untethered Submersible Technology, Durham, New Hampshire, USA, 1999, pp. 1–7.

[5] J. Vaganay, J. Bellingham, J. Leonard, Comparison of fix computation and filtering for autonomous acoustic navigation, Int. J. of Systems Science 29 (10) (1998) 1111–1122.

[6] J. Kinsey, L. Whitcomb, Preliminary field experience with the DVLNAV integrated navigation system for oceanographic submersibles, Control Engineering Practice 12 (12) (2004) 1541–1548.

[7] T. Johansen, T. Fossen, G. Goodwin, Three-stage filter for position estimation using pseudorange measurements, IEEE Transactions on Aerospace and Electronic Systems 52 (4) (2016) 1631–1643.

[8] E. Jørgensen, T. Johansen, I. Schjølberg, Enhanced Hydroacoustic Range Robustness of Three-Stage Position Filter based on Long Baseline Measurements with Unknown Wave Speed, IFAC-PapersOnLine 49 (23) (2016) 61 – 67, 10th IFAC Conference on Control Applications in Marine SystemsCAMS 2016.

[9] B. Stovner, T. Johansen, T. Fossen, I. Schjølberg, Three-stage filter for position and velocity estimation from long baseline measurements with unknown wave speed, in: Proceedings of the 2016 American Control Conference, Boston, USA, 2016, pp. 4532–4538.

[10] J. Jouffroy, J. Opderbecke, Underwater vehicle trajectory estimation using contracting PDE-based observers, in: Proceedings of the 2004 American Control Conf., Vol. 5, Boston, MA, USA, 2004, pp. 4108–4113.

[11] M. Larsen, Synthetic long baseline navigation of underwater vehicles, in: Proceedings of the 2000 MTS/IEEE OCEANS, Vol. 3, Providence, RI, USA, 2000, pp. 2043–2050.

[12] C. LaPointe, Virtual long baseline (VLBL) autonomous underwater vehicle navigation using a single transponder, Master's thesis, Massachusetts Institute of Technology (Jun. 2006).

[13] O. Hegrenas, K. Gade, O. Hagen, P. Hagen, Underwater transponder positioning and navigation of autonomous underwater vehicles, in: Proceedings of the 2009 MTS/IEEE OCEANS, Biloxi, USA, 2009, pp. 1–7.

[14] E. Olson, J. Leonard, S. Teller, Robust Range-Only Beacon Localization, IEEE Journal of Oceanic Engineering 31 (4) (2006) 949–958.

[15] S. Webster, R. Eustice, H. Singh, L. Whitcomb, Preliminary deep water results in single-beacon one-way-travel-time acoustic navigation for underwater vehicles, in: Proceedings of the 2009 IEEE/RSJ International Conference on Intelligent Robots and Systems- IROS 2009, SaintLouis, MO, USA, 2009, pp. 2053–2060.

[16] A. Gadre, D. Stilwell, A complete solution to underwater navigation in the presence of unknown currents based on range measurements from a single location, in: Proceedings of the 2005 IEEE/RSJ International Conference on Intelligent Robots and Systems, Edmonton AB, Canada, 2005, pp. 1420–1425.

[17] P.-M. Lee, B.-H. Jun, K. Kim, J. Lee, T. Aoki, T. Hyakudome, Simulation of an Inertial Acoustic Navigation System With Range Aiding for an

Autonomous Underwater Vehicle, IEEE Journal of Oceanic Engineering 32 (2) (2007) 327–345.
[18] P. Batista, C. Silvestre, P. Oliveira, Single Range Aided Navigation and Source Localization: observability and filter design, Systems & Control Letters 60 (8) (2011) 665–673.
[19] J.-P. Peyronnet, R. Person, F. Rybicki, POSIDONIA 6000: a new long range highly accurate ultra short base line positioning system, in: Proceedings of the 1998 IEEE OCEANS Conference, Nice, France, 1998, pp. 1721–1727.
[20] M. Morgado, P. Batista, P. Oliveira, C. Silvestre, Position USBL/DVL Sensor-based Navigation Filter in the presence of Unknown Ocean Currents, Automatica 47 (12) (2011) 2604–2614.
[21] J. Kinsey, R. Eustice, L. Whitcomb, A Survey of Underwater Vehicle Navigation: Recent Advances and New Challenges, in: Proceedings of the 7th IFAC Conf. on Manoeuvring and Control of Marine Craft, Lisboa, Portugal, 2006.
[22] J. Leonard, A. Bennett, C. Smith, H. Feder, Autonomous underwater vehicle navigation, Tech. Rep. Technical Memorandum 98-1, MIT Marine Robotics Laboratory (1998).
[23] H.-P. Tan, R. Diamant, W. Seah, M. Waldmeyer, A survey of techniques and challenges in underwater localization, Ocean Engineering 38 (14-15) (2011) 1663–1676.
[24] R. Eustice, L. Whitcomb, H. Singh, M. Grund, Experimental Results in Synchronous-Clock One-Way-Travel-Time Acoustic Navigation for Autonomous Underwater Vehicles, in: Proceedings of the 2007 Int. Conference on Robotics and Automation, Rome, Italy, 2007, pp. 4257–4264.
[25] S. Webster, R. Eustice, H. Singh, L. Whitcomb, Advances in single-beacon one-way-travel-time acoustic navigation for underwater vehicles, The International Journal of Robotic Research 31 (8) (2012) 935–950.
[26] D. Yoerger, M. Jakuba, A. Bradley, B. Bingham, Techniques for deep sea near bottom survey using an autonomous underwater vehicle, The International Journal of Robotics Research 26 (1) (2007) 41–54.
[27] P. Batista, C. Silvestre, P. Oliveira, Sensor-based Long Baseline Navigation: observability analysis and filter design, Asian Journal of Control 16 (4) (2014) 974–994.
[28] J. Leonard, R. Rikoski, Incorporation of delayed decision making into stochastic mapping, in: D. Rus, S. Singh (Eds.), Experimental Robotics VII, Vol. 271 of Lecture Notes in Control and Information Sciences, Springer Berlin Heidelberg, 2001, pp. 533–542.
[29] R. Rikoski, Dynamic sonar perception, Ph.D. dissertation, Massachusetts Institute of Technology (Jun. 2003).
[30] M. Stanway, Contributions to Automated Realtime Underwater Navigation, Ph.D. dissertation, Massachusetts Institute of Technology / Woods Hole Oceanographic Institution Joint Program (Feb. 2012).
[31] P. Batista, Long baseline navigation with clock offset estimation and discrete-time measurements, Control Engineering Practice 35 (2015) 43–53.
[32] P. Batista, GES Long Baseline Navigation with Unknown Sound Velocity and Discrete-time Range Measurements, IEEE Transactions on Control Systems Technology 23 (1) (2015) 219–230.
[33] P. Batista, C. Silvestre, P. Oliveira, Pseudo-Range Navigation with Clock Offset and Propagation Speed Estimation, in: Proceedings of the 54th IEEE Conference on Decision and Control, Osaka, Japan, 2015, pp. 7636–7641.
[34] J. Caffery, A new approach to the geometry of TOA location, in: Proceedings of the IEEE VTS Fall VTC2000 52nd Vehicular Technology Conference, Vol. 4, Boston, USA, 2000, pp. 1943–1949.
[35] A. Jazwinski, Stochastic Processes and Filtering Theory, Academic Press, Inc., 1970.
[36] W. Rugh, Linear system theory, 2nd Edition, Prentice-Hall, Inc., 1995.
[37] B. Garau, A. Alvarez, G. Olivier, AUV navigation through turbulent ocean environments supported by onboard H-ADCP, in: Proceedings of the 2006 IEEE Conference on Robotic and Automation, Orlando, FL, USA, 2006, pp. 3556–3561.
[38] O. Hegrenæs, O. Hallingstad, Model-Aided INS With Sea Current Estimation for Robust Underwater Navigation, IEEE Journal of Oceanic Engineering 36 (2) (2011) 316–337.
[39] H. L. Van Trees, K. L. Bell, Bayesian Bounds for Parameter Estimation and Nonlinear Filtering/Tracking, IEEE Press, Piscataway, New Jersey, USA, 2007.
[40] A. Gelb, Applied Optimal Filtering, The MIT Press, 1974.

A. Dynamics of the pseudo-range differences

To compute the dynamics of the pseudo-range differences, take (11) at the discrete-time instant $k+1$, which gives

$$\begin{aligned} r_i^2(k+1) - r_j^2(k+1) = &-2\left(\mathbf{s}_i - \mathbf{s}_j\right)\cdot \mathbf{x}_1(k+1) \\ &+\left(\|\mathbf{s}_i\|^2 - \left\|\mathbf{s}_j\right\|^2\right) x_3(k+1) \\ &+2\left[r_i(k+1) - r_j(k+1)\right] x_4(k+1) \end{aligned} \tag{39}$$

for all $i, j \in \{1, \ldots, L\}$, $i \neq j$. Next, substitute the system dynamics (7) in (39), which gives

$$\begin{aligned} r_i^2(k+1) - r_j^2(k+1) = &-2\left(\mathbf{s}_i - \mathbf{s}_j\right)\cdot \mathbf{x}_1(k) \\ &-2T\left(\mathbf{s}_i - \mathbf{s}_j\right)\cdot \mathbf{x}_2(k) \\ &-2\left(\mathbf{s}_i - \mathbf{s}_j\right)\cdot \mathbf{u}(k) x_3(k) \\ &+\left(\|\mathbf{s}_i\|^2 - \left\|\mathbf{s}_j\right\|^2\right) x_3(k) \\ &+2\left[r_i(k+1) - r_j(k+1)\right] x_4(k) \end{aligned} \tag{40}$$

for all $i, j \in \{1, \ldots, L\}$, $i \neq j$. Now, adding and subtracting $2\left[r_i(k) - r_j(k)\right] x_4(k)$ to the right side of (40) and using (11) gives

$$\begin{aligned} r_i^2(k+1) - r_j^2(k+1) = &-2T\left(\mathbf{s}_i - \mathbf{s}_j\right)\cdot \mathbf{x}_2(k) \\ &-2\left(\mathbf{s}_i - \mathbf{s}_j\right)\cdot \mathbf{u}(k) x_3(k) \\ &+2\left(\left[r_i(k+1) - r_i(k)\right] - \left[r_j(k+1) - r_j(k)\right]\right) x_4(k) \\ &+r_i^2(k) - r_j^2(k) \end{aligned} \tag{41}$$

for all $i, j \in \{1, \ldots, L\}$, $i \neq j$. Finally, using $a^2 - b^2 = (a+b)(a-b)$ in (41) twice gives (13).